Biological nitrate transport in sediments on the Peruvian margin mitigates benthic sulfide emissions and drives pelagic N loss during stagnation events

A.W. Dale, S. Sommer, U. Lomnitz, A. Bourbonnais, K. Wallmann

PII: S0967-0637(15)30130-8
DOI: http://dx.doi.org/10.1016/j.dsr.2016.02.013
Reference: DSRI2596

To appear in: *Deep-Sea Research Part I*

Received date: 28 September 2015
Revised date: 1 February 2016
Accepted date: 23 February 2016

Cite this article as: A.W. Dale, S. Sommer, U. Lomnitz, A. Bourbonnais and K. Wallmann, Biological nitrate transport in sediments on the Peruvian margin mitigates benthic sulfide emissions and drives pelagic N loss during stagnation events, *Deep-Sea Research Part I,* http://dx.doi.org/10.1016/j.dsr.2016.02.013

Biological nitrate transport in sediments on the Peruvian margin mitigates benthic sulfide emissions and drives pelagic N loss during stagnation events

A. W. Dale[1]*, S. Sommer[1], U. Lomnitz[1], A. Bourbonnais[2], K. Wallmann[1]

[1] GEOMAR Helmholtz Centre for Ocean Research Kiel, Wischhofstrasse 1–3, 24148 Kiel, Germany
[2] School for Marine Science and Technology, University of Massachusetts Dartmouth, New Bedford, USA

* Corresponding author: email: adale@geomar.de, Tel. +49–431–600–2291, Fax +49–431–600–2928

ABSTRACT

Benthic N cycling in the Peruvian oxygen minimum zone (OMZ) was investigated at ten stations along 12°S from the middle shelf (74 m) to the upper slope (1024 m) using in situ flux measurements, sediment biogeochemistry and modelling. Middle shelf sediments were covered by mats of the filamentous bacteria *Thioploca* spp. and contained a large 'hidden' pool of nitrate that was not detectable in the porewater. This was attributed to a biological nitrate reservoir stored within the bacteria to oxidize sulfide to sulfate during 'dissimilatory nitrate reduction to ammonium' (DNRA). The extremely high rates of DNRA on the shelf (15.6 mmol m^{-2} d^{-1} of N), determined using an empirical steady-state model, could easily supply all the ammonium requirements for anammox in the water column. The model further showed that denitrification by foraminifera may account for 90% of N_2 production at the lower edge of the OMZ. At the time of sampling, dissolved oxygen was below detection limit down to 400 m and the water body overlying the shelf had stagnated, resulting in complete depletion of nitrate and nitrite. A decrease in the biological nitrate pool was observed on the shelf during fieldwork concomitant with a rise in porewater sulfide levels in surface sediments to 2 mM. Using a non-steady state model to simulate this natural anoxia experiment, these observations were shown to be consistent with *Thioploca* surviving on a dwindling intracellular nitrate reservoir to survive the stagnation period. The model shows that sediments hosting *Thioploca* are able to maintain high ammonium fluxes for many weeks following stagnation, potentially sustaining pelagic N loss by anammox. In contrast, sulfide emissions remain low, reducing the economic risk to the Peruvian fishery by toxic sulfide plume development.

1. INTRODUCTION

The marine nitrogen (N) cycle is an integral component of the biological pump and a major control on atmospheric carbon dioxide concentrations (Gruber, 2004). Quantification of the sources (N_2 fixation) and sinks (denitrification) of bioavailable (fixed) N is thus critical for predicting the evolution of Earth's climate (Galbraith et al., 2004). The most recent estimates suggest that the largest N sink in the ocean today is denitrification in sediments (ca. 100 to 200 Tg N yr^{-1}), with pelagic denitrification including anammox accounting for around one-half of this value (Bianchi et al., 2012; Bohlen et al., 2012; Eugster and Gruber, 2012; DeVries et al., 2013; Somes et al., 2013). Most denitrification in the water column takes place where oxygen concentrations are below ca. 5 μM, that is, in the ocean's oxygen minimum zones (OMZ) of the Eastern Tropical North and South Pacific and the Arabian Sea (Devol et al., 2004; Lam and Kuypers, 2011). By contrast, benthic denitrification occurs worldwide because sediments quickly turn anoxic below the surface oxidized layer (typically a few mm thick on continental margins). Astonishingly, though, empirical relationships derived from global datasets estimate that OMZ sediments, which cover only 1% of the seafloor, may account for 10% of global benthic denitrification (Bohlen et al., 2012). This number is likely to increase if ongoing expansion of the major OMZs continues (Stramma et al., 2008). Hence, there is a real need to more clearly define the pathways and rates of benthic N turnover in these settings.

This need is driven by the discovery of new processes and organisms in oxygen-deficient environments that alter the classical view of benthic N cycling (Fig. 2). Perhaps most significantly, mats of the filamentous chemolithoautotrophic sulfur bacteria *Thioploca* spp. cover vast areas of the continental shelf off Peru and Chile where anoxic bottom waters impinge on the seafloor (Gallardo, 1977; Thamdrup and Canfield, 1996). These bacteria take up large quantities of nitrate (NO_3^-) from the bottom water and store it within intracellular vacuoles at concentrations up to 500 mM (Fossing et al., 1995). The NO_3^- is used as an electron acceptor during the acquisition of energy. Early investigations on the ability of *Thioploca* to denitrify NO_3^- to nitrogen gas (N_2) were inconclusive (Fossing et al., 1995; Otte et al., 1999). Experiments have since shown that *Thioploca* perform dissimilatory nitrate reduction to ammonium (NH_4^+), DNRA (Otte et al., 1999; Zopfi et al., 2001; Høgslund et al., 2009):

$$HS^- + NO_3^- + CO_2 + 2\ H_2O \rightarrow SO_4^{2-} + NH_4^+ + HCO_3^- \quad (1)$$

where free sulfide (HS^-) in porewater is the electron donor that is oxidized by their intracellular, or biological, NO_3^- pool. Note that this reaction is not to be confused with heterotrophic DNRA, which is performed by different bacteria using other electron donors (Thamdrup, 2012). Their micro-aerophilic nature and dependence on sulfide explains why *Thioploca* are found in organic-rich OMZ muds displaying high rates of sulfate reduction (Ferdelman et al., 1997; Høgslund et al., 2009). Yet, paradoxically, *Thioploca* are inhibited by sulfide concentrations of 500 μM or less (Maier and

Gallardo, 1984; Huettel et al., 1996). They overcome this problem by gliding between the sediment surface (to access NO_3^-) and the underlying layers (to access sulfide) within gelatinous sheaths at speeds of up to 10 cm d^{-1} (Jørgensen and Gallardo, 1999). The stored NO_3^- provides the energy to make the journey up and down the sediment and maintain sulfide concentrations within the upper 10 – 20 cm at micromolar levels (Ferdelman et al., 1997; Bohlen et al., 2011).

Thioploca are of broad ecological interest because they conserve fixed N within the benthic environment (NO_3^- reduction to NH_4^+) and at the same time act as an effective barrier to sulfide emissions to the water column. Furthermore, the NH_4^+ produced by DNRA in the sediments contributes to N loss in the water column via anammox (Lam et al., 2009). However, bottom water intrusions of oxygen or depletion of NO_3^- can strongly modulate *Thioploca* community dynamics (Schulz et al., 2000; Gutiérrez et al., 2008). Vacuolated bacteria such as *Thioploca* may overcome periods of NO_3^- depletion by relying on their internal reservoir as their sole source of oxidizing power (Schulz and Jørgensen, 2001). To our knowledge, this has not been demonstrated for *Thioploca* in the field. Yet, it would be an important consideration for the benthic N budget as well as for local fisheries if toxic sulfide is eventually released to the water column.

A second process discovered more recently is denitrification by foraminifera (Risgaard-Petersen et al., 2006). These are unicellular eukaryotes typically <1 mm in diameter commonly found in low-oxygen environments (Levin, 2003). Like *Thioploca*, some species are able to store NO_3^- internally at concentrations approaching 400 mM (Risgaard-Petersen et al., 2006; Piña-Ochoa et al., 2010). Unlike *Thioploca*, however, the NO_3^- is denitrified to N_2, either by the foraminifera themselves or by prokaryotic endobionts (Bernhard et al., 2012). Thus, in contrast to DNRA, these protists alongside denitrifying and ammonium oxidizing (anammox) prokaryotes actively contribute to fixed N loss. Moreover, their motility gives them a competitive advantage by allowing more easy access to the oceanic NO_3^- pool. Theoretical calculations suggest that denitrification by foraminifera could account for almost all of benthic N loss at certain localities on the Peruvian margin (Glock et al., 2013). Similar results have been reported for other regions (Høgslund et al., 2008; Piña-Ochoa et al., 2010; Prokopenko et al., 2011; Bernhard et al., 2012). These studies plainly highlight the knowledge gaps in the global N cycle that need to be taken seriously.

The ecology of *Thioploca* and foraminifera and their potential impact on the N cycle in oxygen-deficient settings is truly remarkable. We developed an empirical steady state diagenetic model to quantify biological NO_3^- transport and reduction in sediments at ten sites on the Peruvian margin within the Humboldt Current upwelling system. Upwelling of nutrient–rich Equatorial Subsurface Water leads to high rates of primary productivity (1.8 – 3.6 g C m^{-2} d^{-1}) and the development of an extensive and perennial OMZ (Pennington et al., 2006). At the time of sampling, however, bottom waters down to 100 m had stagnated and become depleted in NO_3^- and NO_2^- due to sluggish hydrodynamic transport and renewal. This unexpected, yet fortuitous, natural anoxia experiment allowed us to further address additional outstanding questions using a simplified non-steady state

version of the same model: (i) Does the temporal absence of bottom water NO_3^- on the shelf have an impact on bacterial NO_3^- storage and porewater sulfide levels? (ii) What are the linkages between NO_3^- storage, benthic sulfide emissions and water column N loss?

This paper is a companion to Dale et al. (2015) which describes measured and modeled organic carbon fluxes and burial efficiencies at the same stations, and to Sommer et al. (submitted) which presents the benthic N fluxes used to constrain the model.

2. DESCRIPTION OF SAMPLING AREA

The present study area (12°S) falls with the region of maximum upwelling and primary productivity (Quiñones et al. 2010). The mean depth of the OMZ in coastal waters at this latitude is 50 m (Gutiérrez et al., 2008). The shelf stations are strongly affected by annual and inter-annual fluctuations in bottom water redox conditions (Gutiérrez et al., 2008; Scholz et al., 2011). Sampling took place in austral winter when the upwelling intensity is greatest (Morales et al., 1999). Dissolved O_2 concentrations in the bottom water were below the analytical detection limit of the Winkler titration (5 µM) on the shelf down to ca. 420 m which marks the lower edge of the OMZ (Dale et al., 2015). Concentrations of dissolved NO_3^- and NO_2^- were negligible at the shallowest shelf stations at the time of sampling due to restricted circulation (Sommer et al., submitted and Fig. 1). Below 100 m, NO_3^- increased steadily in the OMZ to a maximum of 45 µM. NO_2^- concentrations were also elevated in the OMZ peaking at 9.4 µM at ca. 200 m with a smaller secondary maximum of 7 µM at 350 m. We measured high benthic sulfide emissions up to 14 mmol m^{-2} d^{-1} at the shallowest station where NO_3^- and NO_2^- were absent, although concentrations of free hydrogen sulfide in ambient bottom waters were around the analytical detection limit of 1 µM (Sommer et al., submitted).

The sediments down to ca. 300 m were covered by centimeter-thick mats of the filamentous sulfide oxidizing bacteria *Thioploca* spp. within dense gelatinous sheaths (Henrichs and Farrington, 1984; Gutiérrez et al., 2008; Dale et al., 2015). The surface coverage by bacterial mats was 100% at the shallowest sites, decreasing to roughly 50% at 300 m where the bacteria formed patches several decimeters in diameter. *Thioploca* trichomes extended into the overlying water by 1 – 2 cm (c.f. Huettel et al., 1996) and were visible down a depth of ca. 20 cm at all stations with mats. The sediments are highly reducing gelatinous cohesive muds releasing large amounts of dissolved ammonium, iron and phosphate to the water column (Bohlen et al., 2011; Scholz et al., 2011; Noffke et al., 2012). The presence of mats on the middle shelf despite the absence of bottom water NO_3^- implies that the system was transitioning toward a sulfidic regime, where *Thioploca* completely disappear and the biomass becomes dominated by nematodes (Gutiérrez et al., 2008).

No mats were visible on the upper slope at the deepest station in the OMZ (St. 8, 409 m). The sediment here was hard grey clay underlying a 2 – 3 cm porous surface layer containing large numbers of live nitrate-storing foraminifera (ca. 4×10^5 individuals / 50 cm^2, J. Cardich, unpub. data). Similar

foraminiferal 'sands' were described for 11°S in areas where the slope angle becomes critical for internal wave breaking on the seafloor (Mosch et al., 2012). Current-induced sediment reworking and winnowing favors the formation of phosphorite nodules that were also observed here (c.f. Glenn and Arthur, 1988). Foraminifera abundances ranging from 38×10^4 to 64×10^4 individuals / 50 cm^2 were measured elsewhere in the OMZ, whereas below the OMZ the abundance was two orders-of-magnitude lower (J. Cardich, unpub. data).

Dale et al. (2015) characterized the Peruvian margin at 12 °S into three zones reflecting bottom water O_2 levels and sedimentary POC content: (i) the middle and outer shelf (< ca. 200 m, 5 to 10% POC, O_2 < detection limit (dl, 5 μM) during sampling) where non-steady state conditions are occasionally driven by intrusion of oxygenated bottom waters (Levin et al., 2002; Gutiérrez et al., 2008), (ii) the core of the OMZ (ca. 200 to 450 m, 10 – 20% POC, O_2 < dl), and (iii) the deep stations on the slope below the OMZ (≤ ca. 5% POC and O_2 > dl). We adopt the same notation in this work.

3. MATERIAL AND METHODS

3.1. Sampling and geochemical analysis

Sedimentary and benthic flux data are presented from 10 sampling stations (Table 1) visited during expedition M92 on RV Meteor in January/February 2013 (austral summer, low upwelling season). Data were obtained using multi–corers (MUC) and benthic landers (Biogeochemical Observatories or BIGO). Complete details of the lander deployments and benthic flux measurements are provided by Sommer et al. (submitted) and Dale et al. (2015). The uncertainty in the measured fluxes was calculated from the standard error of the slope of the concentration versus time data points. The full set of concentration time series data is provided elsewhere (Sommer et al., submitted).

Samples for sediment and porewater analysis were taken using both MUC and BIGO technologies. We report on MUC data only since the core length (ca. 20 – 40 cm) was typically much greater than the BIGO cores (ca. 10 cm) and less prone to handling artifacts. The sediments sampling resolution was 0.5 cm in the upper 5 cm, increasing to 3 to 4 cm at the bottom of the core. Details on sample handling and processing are described in Sommer et al. (submitted) and Dale et al. (2014, 2015).

Solutes measured include ammonium (NH_4^+), nitrite (NO_2^-), dissolved ferrous iron (Fe^{2+}), phosphate (PO_4^{3-}) and sulfide (H_2S). Results for Fe^{2+} and PO_4^{3-} are reserved for a separate manuscript. These analytes were measured onboard using standard photometric techniques with a Hitachi U2800 photometer (Grasshoff et al., 1983). Aliquots of porewater were diluted with O_2–free artificial seawater prior to analysis. Porewater samples for Fe^{2+} analysis were treated with ascorbic acid directly after filtering (0.2 μm) inside the glove bag. Detection limits for NO_3^-, NH_4^+ and H_2S were 1 μM, 5 μM for PO_4^{3-} and 0.1 μM for NO_2^-. Total alkalinity (TA) was determined onboard by direct titration of 1 ml porewater with 0.02 M HCl using a mixture of methyl red and methylene blue as indicator and

bubbling the titration vessel with Ar gas to strip CO_2 and H_2S. The analysis was calibrated using IAPSO seawater standard, with a precision and detection limit of 0.05 meq l^{-1}. Ion chromatography (Methrom 761) was used to determine sulfate (SO_4^{2-}) in the onshore laboratory with a detection limit of < 100 µM and precision of 200 µM. Major cations were determined by ICP-AES with precision and relative accuracy as given by Haffert et al. (2013). Analytical details of dinitrogen gas (N_2) measurements are described by Sommer et al. (unpub. data).

Samples were analyzed for POC, particulate organic nitrogen (PON) and total particulate sulfur as described by Dale et al. (2014), with a precision and detection limit of 0.04 and 0.05 dry weight percent (%), respectively.

Additional sediment cores were taken from selected shelf and OMZ stations for the determination of total NO_3^- and NO_2^- in the sediment. The upper 10 cm were sliced in 1 – 2 cm intervals, repeatedly frozen and thawed to burst intracellular vacuoles of *Thioploca* and foraminifera and then centrifuged at 3000 g for 20 min. Analysis of the filtered porewater gives the biological NO_3^- (and NO_2^-) stored within vacuolated organisms as well as any porewater NO_3^- and NO_2^- present (e.g. Dale et al., 2009; Lichtschlag et al., 2010). Although the contribution of *Thioploca* and foraminifera to the total NO_3^- pool was not quantified experimentally, their rates of NO_3^- consumption were estimated using the diagenetic model (see below). In what follows, biological NO_3^- (termed 'BNO_3^-') refers to the total concentration NO_3^- + NO_2^- minus the porewater concentration measured following centrifugation without freezing.

3.2. Numerical modeling

3.2.1. Model architecture

A steady state 1–D numerical reaction–transport model was developed to simulate the biogeochemical cycling in surface sediments (upper 30 to 100 cm). Effort was focused on simulating N turnover rates using three independent data sources to constrain the model: (i) porewater distributions, (ii) benthic fluxes of dissolved N species and O_2 at the deeper stations, and (iii) dissolved inorganic carbon (DIC) fluxes calculated from TA and pCO_2 concentrations. The latter have been reported by Dale et al. (2015) and are assumed to be equivalent to total benthic respiration rates. Benthic fluxes are an important constraint on N cycling in the model because processes such as denitrification and nitrification occur in the surface sediment layers that are not adequately resolved by the porewater sampling resolution (≥ 0.5 cm). The model is essentially identical to that applied by Bohlen et al. (2011) to data from a transect at 11°S. A full description of the model can be found in that publication and in the Supplement whilst modifications are explained below.

In total, 14 solutes were considered including O_2, NO_3^-, NO_2^-, NH_4^+, N_2, H_2S, PO_4^{3-}, SO_4^{2-}, Fe^{2+}, DIC and CH_4. At selected stations, we also considered intracellular NO_3^- in foraminifera, $NO_{3\ for}^-$. The

current version of the model does not treat pH explicitly, such that modeled H_2S and DIC represent the sum of total dissolved sulfide and inorganic carbon, respectively. Solid species considered were POC, PON, adsorbed NH_4^+ ($NH_4^+{}_{ads}$), reactive iron oxide (FeOOH) and particulate sulfur (PS). Chemical compounds were transported by molecular diffusion (for solutes) and sediment burial (for solutes and solids). At stations with oxic bottom waters, sediment mixing by fauna (bioturbation) and non–local transport of solutes by burrowing organisms (bioirrigation) was also considered. Solute and solid concentrations were modeled in units of mmol cm^{-3} of porewater and dry weight percent (wt–%), respectively, except for $NH_4^+{}_{ads}$ (mmol g^{-1}).

The modeled reaction network and rate expressions are summarized from Bohlen et al. (2011) (see Supplement). The degradation of particulate organic matter (POM) forms the basis of the biogeochemical cycling in the model. POM is defined chemically as $(CH_2O)(NH_3)_{rNC}$, where r_{NC} is the measured atomic N:C ratio (mol N / mol C). POM was degraded by aerobic respiration, denitrification, iron oxide reduction, sulfate reduction and methanogenesis. DIC is produced by POC degradation only because carbonate dissolution and precipitation amount to < 5% of benthic DIC fluxes (Dale et al., 2015).

A schematic overview of the modeled N cycle is shown in Fig. 2. Organic nitrogen was released as NH_4^+ during POM mineralization (ammonification). Adsorption of NH_4^+ onto sediment particles was controlled by an empirical equilibrium constant, K_{NH4} (Mackin and Aller, 1984). Canonical denitrification (reduction of NO_3^- to N_2) was modeled as a two–step process with NO_2^- as a reactive intermediate. Minor intermediates such as NO and N_2O were not considered due to order-of-magnitude lower concentrations compared to NO_2^- (Thamdrup, 2012). Anammox is included, but symbiotic interactions between *Thioploca* and ammonium oxidizing bacteria proposed in a previous study are not (Prokopenko et al., 2006). Similarly, nitrification was described as the stepwise oxidation of NH_4^+ to NO_2^- to NO_3^-. NO_2^- produced by these pathways was available for anammox that shunts NO_2^- and NH_4^+ into N_2 gas. Preliminary simulations with denitrification coupled to Fe^{2+} oxidation (Straub et al., 1996) showed that this process was of minor importance and so the rate constant for this reaction was set to zero. NO_3^- consumption by chemotrophic DNRA is described in section 3.2.3.

The major differences between the present model and the former one (Bohlen et al., 2011) lie in the treatment of DNRA. Bohlen et al. (2011) explicitly modeled intracellular NO_3^- and NO_2^- transport into the sediment by sulfide oxidizing bacteria. In this study, we imposed the depth-dependent rate of DNRA directly, such that the uptake of intracellular NO_3^- is implicitly calculated as the depth-integrated rate of DNRA. NH_4^+ is produced in the sediment depending on the DNRA rate at each sediment depth. We adopted this approach because it allows more flexibility to simulate bacterial NO_3^- transport and reduction. The rate-depth profiles of DNRA are given in the Supplement.

Secondly, Bohlen et al. (2011) allowed DNRA to proceed using both NO_3^- and NO_2^- as electron acceptors at the shallow shelf station (their St. 1). This was done because shelf bottom waters at 11°S were enriched in NO_2^- and *Thioploca* have been observed to display positive chemotactic behavior

toward NO_2^- in laboratory experiments (Zopfi et al., 2001). Bottom water NO_2^- concentrations were also high on the shelf at 12°S (Sommer et al., submitted) and we measured high NO_2^- in some, but not all, of the freeze/thaw experiments. Yet, it remains to be shown whether this intracellular NO_2^- was taken up by the bacteria directly from the bottom water or whether it is the result of stepwise intracellular reduction of NO_3^- to NH_4^+ (Otte et al., 1998; Zopfi et al., 2001; Høgslund et al., 2009). For the sake of parsimony, we assume here that it reflects the latter, meaning that the sole source of oxidized N for DNRA in our modified model is NO_3^- from the bottom water.

We also considered biological NO_3^- transport by foraminifera. The exact mechanism of the N loss pathway is unimportant for the macro-scale (cm) simulations performed here, that is, denitrification by the foraminifera or by their prokaryotic symbionts (Bernhard et al., 2012). During our fieldwork at 12°S, live foraminifera were abundant and visible to the naked eye mainly within the OMZ (J. Cardich, unpub. data). This was especially obvious at St. 8 (409 m) where bacterial mats were absent and the abundance of foraminifera gave the appearance of the aforementioned 'foraminiferal sand' (Dale et al., 2015). Many of the species identified on the Peru margin are capable of heterotrophic denitrification (Risgaard-Petersen et al., 2006; Cardich et al., 2012), summarized as:

$$CH_2O(NH_3)_{rNC} + 0.8NO_3^- \rightarrow 0.4\ N_2 + r_{NC}\ NH_4^+ + HCO_3^- + 0.4\ H_2O + (0.2 - r_{NC})\ H^+ \quad (2)$$

We modified the model to include intracellular NO_3^- in foraminifera, $NO_{3\,for}^-$, at selected stations. Foraminifera are motile and use their pseudopodal network to facilitate access to NO_3^- at the sediment surface (Koho et al., 2011). Biological NO_3^- transport by foraminifera was formulated as a non-local exchange process analogous to bioirrigation (see Supplement). Since the NO_3^- reservoir is confined to the cells, molecular diffusion of $NO_{3\,for}^-$ was set to zero. The rate of denitrification by foraminifera was formulated as R_{for} (mmol C cm^{-3} d^{-1}):

$$R_{for} = R_{POC} \cdot \frac{[NO_{3\,for}^-]}{[NO_{3\,for}^-] + K_{for}} \quad (3)$$

where R_{POC} is the rate of POC mineralization and K_{for} is a model-fitted half-saturation concentration for this process. It is not unreasonable to assume that foraminifera have a competitive advantage over non-motile bacteria by actively seeking out fresh organic matter in the sediment (Risgaard-Petersen et al., 2006; Koho et al., 2011). The other carbon respiration pathways were thus inhibited by foraminifera by multiplying the reaction rates by K_{for} / (K_{for} + $[NO_{3\,for}^-]$). The total rate of POC degradation is equal to the sum of the primary carbon oxidation pathways plus R_{for} (see Supplement).

At all stations, we allowed precipitated sulfur to be oxidized anaerobically using NO_3^- (Schippers and Jørgensen, 2002). In what follows, we apply the term 'denitrification' to the sum of N_2 production via this pathway and denitrification (NO_2^- reduction to N_2).

Finally, due to the depletion of SO_4^{2-} on the middle shelf (St. 1), the current model includes methanogenesis and anaerobic oxidation of methane (AOM). The latter consumes sulfate and methane leading to production of sulfide and bicarbonate (Barnes and Goldberg, 1976):

$$SO_4^{2-} + CH_4 + CO_2 \rightarrow H_2S + 2HCO_3^- \quad (4)$$

3.2.2. Constraints on the N cycle

N turnover rates were estimated by inversely fitting the model to measured porewater profiles and benthic fluxes, as outlined in Bohlen et al. (2011). In brief, the measured NH_4^+ concentrations are treated as a major constraint on the rate of organic matter degradation. However, other reactions also affect the NH_4^+ concentration, such as DNRA, nitrification of NH_4^+ by O_2 and NO_2^- (anammox) and adsorption onto particles. The net rate of NH_4^+ accumulation at depth is thus determined from the sum of NH_4^+ producing and consuming reactions as well as transport pathways.

The rate of organic matter mineralization was estimated by first fitting a continuous exponential-type function through the measured NH_4^+ concentrations at each station to obtain a best-fit concentration profile of observed NH_4^+ ($NH_4^+{}_{OBS}$). The rate of ammonification at each depth in the sediment, R_{AMF}, was then determined from the rates, R, of pathway *j*, (R_j, Fig. 2):

$$R_{AMF} = k_{fit} \times (NH_4^+{}_{OBS} - NH_4^+) - \text{DNRA } (R_9) + \text{nitrification } (R_6) + \text{anammox } (R_8) + \text{adsorption } (R_{11}) \quad (5)$$

Once R_{AMF} is known, the rate of POC mineralization, R_{POC}, can be calculated using the measured organic N:C ratio:

$$R_{POC} = R_{AMF} / r_{NC.} \quad (6)$$

The first term on the right-hand-side in Eq. (5) describes how the modeled NH_4^+ concentration is fit to the observed concentration function at each time step using a kinetic constant, k_{fit} (yr^{-1}). k_{fit} was prescribed a high value to ensure that the modeled concentrations were maintained at the measured values. The remaining reactions on the right produce and/or consume NH_4^+. The determination of R_{AMF} thus requires knowledge of the rates of nitrification, anammox, DNRA and NH_4^+ adsorption. Nitrification rates are low in this setting (Bohlen et al., 2011) and the rate constant for this reaction was assumed to be invariable across the transect (Table S3). Similarly, adsorption of NH_4^+ was calculated from a constant equilibrium adsorption coefficient of 1.6 (Mackin and Aller, 1984). The rates of anammox and DNRA were, however, adjusted to fit the data. These processes have opposing impacts on porewater NH_4^+ concentration (i.e. consumption versus production). As a result of Eq. (5),

their magnitude determines the amount of NH_4^+ that needs to be produced from ammonification in order to maintain a close fit between observed and modeled NH_4^+ concentration. For example, anammox consumes NH_4^+ and high rates of this process will stimulate ammonification in order to maintain a fit to the NH_4^+ profile (the opposite is true for DNRA). At the same time, ammonification is coupled to organic carbon degradation through Eq. (6), meaning that anammox indirectly increases TA and decreases SO_4^{2-} since sulfate reduction is the major carbon degradation pathway on the margin (Fossing, 1990; Bohlen et al., 2011). Conversely, DNRA will decrease the rate of organic matter degradation and lead to less accumulation of TA and depletion of SO_4^{2-}. Hence, TA and SO_4^{2-} concentrations provide a further constraint on the rates of DNRA and anammox. Furthermore, the benthic fluxes of NO_3^-, NO_2^- and N_2 across the sediment-water interface will also be strongly influenced by the rates of DNRA, anammox and organic matter degradation. The rate of organic matter degradation is also intimately linked to the DIC flux which is calculated from pCO_2 and TA measurements in the benthic chambers (Dale et al., 2015). Thus, multiple data sources are used to determine the rates of N turnover. Note that heterotrophic denitrification (R_3) is implicitly solved during this procedure since it is directly coupled to organic matter degradation.

Foraminiferal denitrification was simulated at stations where denitrification and anammox were insufficient to drive the measured N_2 fluxes. In practice, this applied to St. 5 (195 m), 6 (244 m), 7 (306 m) and St. 8 (409 m) only. At the shallower shelf stations, N_2 fluxes were very low and foraminiferal denitrification was not considered. At deeper oxygenated stations, denitrification by foraminifera was not considered since their abundance was at least two orders-of-magnitude lower than in the OMZ (Glock et al., 2013; J. Cardich, unpub. data). No attempt was made to relate foraminiferal abundances with denitrification because cell-specific rates were not measured.

3.2.3. Steady state limitations

The rate of organic matter degradation is constrained by the benthic DIC flux as well as porewater profiles of NH_4^+, SO_4^{2-} and TA, all assumed to be in steady state. Yet, the Peruvian shelf is a dynamic environment where primary production, bottom water redox conditions and *Thioploca* biomass vary due to seasonal and sub-seasonal anomalies in oceanographic conditions (Gutiérrez et al., 2008; Graco et al., 2007; Dale et al., 2015). During our fieldwork, bottom waters on the shelf had stagnated, leading to depletion of NO_3^- and benthic N fluxes that were not balanced (Sommer et al., submitted). This is mostly likely due to temporal decoupling of NO_3^- uptake and reduction by *Thioploca*. Using a non-steady state model developed in the final discussion section of this manuscript, we find that the error in the simulated rates and fluxes using a steady state approach is around 30 to 50 %.

4. RESULTS AND DISCUSSION

4.1. Organic carbon and nitrogen mineralization

The model shows excellent agreement with the porewater data and DIC fluxes at all stations, which indicates that the POC degradation rates are simulated accurately (Fig. 3). POC mineralization rates and DIC fluxes increase from ca. 2 mmol m^{-2} d^{-1} below the OMZ to 66 mmol m^{-2} d^{-1} at St 1 on the middle shelf (Dale et al., 2015). Sulfate reduction accounts for >95% of POC mineralization in sediments covered by sulfide-oxidizing *Thioploca*-mats (Table S5). The derived rates are similar to those determined previously for sediments with *Thioploca* (Fossing, 1990; Ferdelman et al., 1997; Thamdrup and Canfield, 1996; Bohlen et al., 2011).

The high mineralization rates on the middle shelf are further reflected in the rapid accumulation of porewater NH_4^+ and TA and depletion of SO_4^{2-} (Fig. 3). The NH_4^+ is partly produced by ammonification of PON at maximum rates of 6.5 mmol m^{-2} d^{-1} (Table 2). This is a minor fraction of the measured NH_4^+ flux which surpasses 20 mmol m^{-2} d^{-1} (Table 2 and Fig. 4). The shortfall is supplied by *Thioploca* performing DNRA (see Section 4.2).

Sediments on the middle shelf sampled with a longer gravity core revealed that SO_4^{2-} was completely consumed at approximately 60 – 70 cm below the sea floor where methane begins to accumulate (Maltby et al., 2015). At this interface, sulfate reduction is coupled to AOM (Barnes and Goldberg, 1976). The SO_4^{2-} concentration gradient implies that AOM consumes 2 mmol m^{-2} d^{-1} of SO_4^{2-}, which represents only a few percent of total sulfate reduction. The downward flux of calcium and magnesium cations at this station equals 0.7 mmol m^{-2} d^{-1}, indicating that around 35 % of the DIC produced by AOM (Eq. (4)) is precipitated as authigenic carbonates (Dale et al., 2015).

High mineralization rates on the middle shelf are driven by high POC rain rates (Dale et al., 2015). However, the organic fraction is diluted by terrestrial inorganic material, giving relatively low POC and PON content compared to the outer shelf and OMZ (Fig. 3). Surface POC and PON content increase in the OMZ to maximum values of 17% and 2%, respectively. These are typical for the Peruvian margin and result from organic matter preservation under low oxygen bottom waters (Suess, 1981; Dale et al., 2015). The model does not capture the transient increase in POC and PON at 15 cm depth at the OMZ stations caused by climatic shifts at the end of the Little Ice Age ca. 1820 AD (discussed by Dale et al., 2015). Average C:N ratios in the upper 10 cm increased from 9.3 to 12.2 between the shallowest to the deepest stations, as shown previously (Henrichs and Farrington, 1984; Gutiérrez et al., 2009). This is driven by deposition of older, reworked POC from sites higher up on the slope (Dale et al., 2015).

4.2. Evidence for biological nitrate transport and reduction by Thioploca

Biological NO_3^- reduction by *Thioploca* can dominate benthic N and S turnover in organic-rich sediments underlying oxygen deficient waters (Jørgensen and Gallardo, 1999; Høgslund et al., 2009).

Although conspicuous *Thioploca* mats provide circumstantial evidence in support of DNRA, additional observations provide compelling evidence for this process. Firstly, on the basis of the in situ fluxes on the middle shelf, Sommer et al. (submitted) showed that NH_4^+ fluxes were a factor of three higher than DIC fluxes when normalized to sediment C:N ratios. They further showed that the NH_4^+ flux could not be supported by the accumulation and mineralization of PON deposited on the seafloor. A sulfate-ammonium property-property plot supports and extends this finding for stations 1 (74 m) to 7 (306 m) where bacterial mats were observed (Fig. 5). The C:N ratio of organic matter undergoing mineralization, r_{CN} (mol C / mol N) , can be estimated by multiplying the slope of the regression curve ($-d\mathrm{NH_4^+}/d\mathrm{SO_4^{2-}} = 0.27$) by the ratio of the diffusion coefficients, D_{NH4}/D_{SO4} (Burdige, 2006):

$$\frac{d\mathrm{NH_4^+}}{d\mathrm{SO_4^{2-}}} \cdot \frac{D_{\mathrm{NH4}}}{D_{\mathrm{SO4}}} = -\frac{1}{r_{\mathrm{CN}} \cdot \mathbb{L}} \qquad (7)$$

where $\mathbb{L}$ is the number of moles of sulfate consumed per mole of organic carbon oxidized, assumed to be 0.5 (Table S3). For the bottom water temperature of 14 °C, $D_{NH4}/D_{SO4} \approx 1.9$ and $r_{CN} \approx 3.9$, implying organic matter enriched in N relative to C. The average measured C:N ratio on the shelf is more than double this value (9.8 ± 0.5, Fig. 3), which indicates that most porewater NH_4^+ is not derived from organic matter. Rates of benthic N_2 fixation to ammonium are very low in comparison to ammonification (Sommer et al., submitted), leaving DNRA as the logical source of the excess NH_4^+.

Secondly, sulfide concentration profiles indicate a large diffusive flux that is entirely consumed at 20 cm depth (Fig. 3). Titration by iron oxyhydroxides cannot explain this since their availability under the highly reducing conditions is limited (Scholz et al., 2011). *Thioploca* were observed down to 20 cm depth in the sediments, which probably marks the limit where they are able to penetrate on a full 'tank' of NO_3^- to seek out sulfide (Schulz et al., 1996; Jørgensen and Gallardo, 1999). Sulfide concentrations from St. 1 are higher and contrast with this idea, as will be discussed later.

Thirdly, biological nitrate (BNO_3^-) concentrations following the freeze-thaw procedure were far in excess of NO_3^- determined in porewater extracted by centrifugation (Fig. 3). At the shallowest station, BNO_3^- was close to 1 mM whereas porewater NO_3^- was below detection limit. In general, at the highly reactive shelf stations, NO_3^- was consumed within the upper 0.5 cm, which corresponds to the sampling resolution. The BNO_3^- pool ranged between 5.3 and 28.2 mmol m^{-2} (Table 3) and tailed off rapidly below 2 cm, which coincides with the base of the *Thioploca* mats. Similar observations elsewhere have been attributed to the release of biologically-stored NO_3^- within vacuolated bacteria (Fossing et al., 1995; Thamdrup and Canfield, 1996; Graco et al., 2001; Zopfi et al., 2001; Lichtschlag et al., 2010; Chong et al., 2012) or foraminifera (Prokopenko et al., 2011, Bernhard et al., 2012). The very low or absent N_2 fluxes on the shelf (Fig. 4) indicates that the BNO_3^- pool originates from *Thioploca* rather than denitrifying foraminifera. At this stage, we cannot rule out that NO_3^- stored

within deposited microalgae, such as diatoms, also contributes to this 'hidden' NO_3^- reservoir (Lomstein et al., 1990).

Finally, the modeled NH_4^+, TA and SO_4^{2-} profiles and the DIC and NH_4^+ fluxes are consistent with DNRA. The modeled rate of DNRA on the middle shelf (15.6 mmol m^{-2} d^{-1}) is amongst the highest value reported for open marine systems and is twice the rate of ammonification (Table 2, Fig. 4) (Huettel et al., 1996; Thamdrup and Canfield, 1996; Graco et al., 2001; Dale et al., 2009; Bohlen et al., 2011; Song et al., 2013). This identifies the sediments as an important recycling depot for fixed N via DNRA. Astonishingly, DNRA can easily cover the NH_4^+ required to sustain pelagic N loss rates by anammox of >10 mmol m^{-2} d^{-1} of N on the shelf (Hamersley et al., 2007; Lam et al., 2009; Kalvelage et al., 2013). The implication is that the benthic microbial community is a catalyst for fixed N loss on the margin, despite conserving fixed N via the DNRA reaction.

It is important to reiterate that no NO_3^- flux was measured on the shelf due to the absence of bottom water NO_3^- (Fig. 1). DNRA was required in the model as a source of NH_4^+ since otherwise mineralization of organic matter would have to supply all the NH_4^+. This entails higher sulfate reduction rates, leading to a stronger accumulation of TA and depletion of SO_4^{2-} than observed (Fig. 3, red curves) and a three-fold increase in DIC flux from 62 to 206 mmol m^{-2} d^{-1}. The simulated NO_3^- influx at St. 1 to 3 therefore represents the *theoretical* steady-state rate of NH_4^+ production via DNRA that is required to simulate the data (Fig. 4), and assumes that the NH_4^+ profile is at steady state. The error in the rates incurred by applying a steady state model to a dynamic system will be quantified using a non-steady state model (Section 4.4).

4.3. Pathways of fixed N loss

The modeled rates of fixed N loss by microbial denitrification and anammox (0.5 – 1.1 mmol m^{-2} d^{-1}, Table 2) are typical for marginal sediments and similar to those at 11°S, with denitrification being generally more important than anammox (Joye and Anderson, 2008; Bohlen et al., 2011). However, N loss at St. 7 (306 m) and St. 8 (409 m) was elevated to 1.5 – 2.4 mmol m^{-2} d^{-1} of N as a result of heterotrophic denitrification by foraminifera. By comparison, N loss in the water column is ca. 3 mmol m^{-2} d^{-1} (Kalvelage et al., 2013), demonstrating that sediments are significant sites in terms of N loss from the whole ecosystem. The sediments at St. 7 and 8 contained an abundance of NO_3^- storing denitrifying foraminifera such as *Bolivina seminuda* and the probable denitrifier *Bolivina costata* (4×10^5 individuals / 50 cm^2, J. Cardich, unpub. data). Highest BNO_3 inventories were also measured at St. 8 where no mats were visible (28.2 mmol m^{-2}, Table 3). According to the model, heterotrophic denitrification by foraminifera accounts for 90% of N_2 production at this station, with a further significant contribution of 62% at St. 7 (Table 2). Our data support the idea that denitrifying foraminifera are major players in the N cycle at Peru (Glock et al., 2013), as observed in other oxygen-

deficient environments (Høgslund et al., 2008; Piña-Ochoa et al., 2010; Prokopenko et al., 2011; Bernhard et al., 2012).

On the shelf, *Bolivina* spp. were also abundant (J. Cardich, unpub. data) in line with previous observations (Glock et al., 2013; Cardich et al., 2012). However, measured N_2 fluxes were negligible (Fig. 4). In contrast to *Thioploca* then, it would appear that foraminifera had already exhausted their internal NO_3^- reservoir following the stagnation event. This is consistent with the longer turnover time of the biological NO_3^- pool of several days-to-weeks for *Thioploca* (see following section) compared to a few days for foraminifera (Høgslund et al., 2008; Bernhard et al., 2012).

No attempt was made to simulate eukaryotic denitrification at St. 5 and 6, despite high N_2 fluxes of 2.0 and 5.6 mmol m^{-2} d^{-1} of N, respectively (Fig. 4), and abundant foraminifera (J. Cardich, unpub. data). This is because there was an excess flux of N_2 from the sediment at these stations of around 3 mmol m^{-2} d^{-1} of N that cannot be captured by a steady state model (Sommer et al., submitted). These authors attributed the imbalance to either a temporal decoupling between NO_3^- uptake and reduction by foraminifera or an artifact triggered by a rapid decrease in electron acceptors inside the benthic incubation chambers at these stations (see Sommer et al., submitted or further discussion).

4.4. Benthic response to bottom water stagnation

Observations of a large biological NO_3^- pool in surface sediments on the shelf along with the absence of NO_3^- in the bottom water demonstrate that *Thioploca* were using their intracellular reserves to survive the stagnation period. Although it is not known for how long *Thioploca* had been deprived of bottom water nitrate (BW-NO_3^-), data from the previous cruise (M91) showed that NO_3^- was absent on the shelf for at least four weeks prior to our sampling (H. Bange, pers. comm.).

We modified the steady state model to test whether the temporal trends in biological NO_3^- and H_2S in shelf sediments could be attributed to water column stagnation, depletion of BW-NO_3^- and a reduction in DNRA (Fig. 3). The simplified model considers organic matter degradation and DNRA only. Biological NO_3^- transport was modeled dynamically by explicitly including the sources and sinks of the intracellular NO_3^- pool (see Supplement). An average POC degradation rate-depth profile based on the highly reactive sites St. 1 and St. 2 was used, equal to ca. 45 mmol m^{-2} d^{-1}.

Consumption of biological NO_3^- was simulated using first-order kinetics, with a rate constant calculated from the observed decrease in the BNO_3^- pool. The depth-integrated BNO_3^- content decreased by one-half from 10.9 to 5.3 mmol m^{-2} within ten days at St. 1 (Table 3), equivalent to a first-order decay constant of around 25 yr^{-1}. A near identical result can be derived for St. 3. This agrees with bottom water nitrate observations that suggest that *Thioploca* could have been reliant on their internal reserves for several weeks before we carried out our sampling.

The model was first run to steady state by specifying a BW-NO_3^- concentration of 25 µM above a 0.4 mm diffusive boundary layer during ventilated periods (Graco et al., 2007). BW-NO_3^- was then

forced to zero over a 9 d period to simulate the onset of a stagnation event, and then maintained at zero levels until a new quasi-steady state was reached (Fig. 6). The boundary BNO_3^- concentration (BNO_3^- *), initially at 6 mM, was scaled to BW-NO_3^-. The simulated rates and fluxes prior to stagnation can be viewed in Fig. 7 and 8. The initial NO_3^- uptake rate by *Thioploca* is 8 mmol m^{-2} d^{-1} whereas NO_3^- diffusion across the diffusive boundary layer is 5 mmol m^{-2} d^{-1} (Fig. 7). NH_4^+ efflux under these conditions is 12 mmol m^{-2} d^{-1} (Fig. 7b). These values approximate benthic N dynamics at times when NO_3^- is available in the bottom water (Bohlen et al., 2011).

The model predicts a H_2S efflux of 12 mmol m^{-2} d^{-1} prior to stagnation. Interestingly, it was not possible to simulate zero H_2S flux with the derived rate constant for DNRA because extremely high rates of sulfate reduction close to the sediment surface lead to an inevitable loss of H_2S by diffusion. This suggests that the *Thioploca* community on the shelf is unable to completely oxidize sulfide during the high productivity season. Sulfide buffering by iron oxyhydroxides can only reduce H_2S emissions by 1 to 2 mmol m^{-2} d^{-1} (Noffke et al., 2012). Furthermore, the maximum flux of NO_3^- across a 0.3 to 0.4 mm-thick diffusive boundary layer above the mats (Huettel et al., 1996) can be calculated to be 7 to 10 mmol m^{-2} d^{-1}. Due to this physical limitation on the NO_3^- flux, sulfide consumption by other nitrate reducing bacteria relying on NO_3^- supply by diffusion would not be able reduce the sulfide flux completely. Enhanced NO_3^- transport into the permeable surface mat structure by advection of bottom water over the sediments (Huettel et al., 1996), or a thinner diffusive boundary layer, could conceivably drive higher rates of bacterial sulfide oxidation, and it would be worthwhile to investigate this further in future.

Benthic fluxes of NO_3^- and BNO_3^- decrease rapidly during stagnation (Fig. 7a). N_2 flux adjusts synchronously with BW-NO_3^- because the diffusive path length between the denitrification sites and the bottom water is very short (< 0.5 cm). The rate of denitrification on the Peru margin should, therefore, be accurately reflected in the N_2 fluxes measured in benthic chambers under transient conditions (compare N_2 flux in Fig. 7a with NO_2^- reduction, R_2, in Fig. 8a). However, > 100 d are required for NH_4^+ flux to relax to a new quasi-steady state at which point NH_4^+ release is solely driven by ammonification (Fig. 7b). This is because (i) NH_4^+ that is produced by DNRA in the upper 10 cm has a longer diffusive path length to the bottom water, and (ii) NH_4^+ continues to be produced from intracellular BNO_3^- for some weeks following stagnation. This can be more clearly appreciated by (i) the slow depletion of porewater NH_4^+ over time (Fig. 9), and (ii) the attenuated rate of DNRA compared to the other pathways (Fig. 8c).

The flux of H_2S increases very rapidly by ca. 3 mmol m^{-2} d^{-1} during stagnation (Fig. 7b) due to a switch in carbon respiration from nitrate and nitrite reduction to sulfate reduction in the uppermost sediment layers. It implies that H_2S emissions on the Peru shelf will initially respond rapidly to a decrease in BW-NO_3^-. Data from the benthic chamber deployments on the outer shelf at St. 3 indeed show that H_2S is immediately released when NO_2^- + NO_3^- fall below 1 µM after 20 h of incubation (Fig. 10). A quasi-steady state flux of ca. 21 mmol m^{-2} d^{-1} is reached when stagnation is fully

established, which is of the same order as the flux of 14 mmol m^{-2} d^{-1} determined at the shallowest station where NO_3^- and NO_2^- were absent (Sommer et al., submitted). Analogous to NH_4^+, the long time required for the H_2S flux to equilibrate can be explained by the fact that, prior to stagnation, DNRA produces a 'deficit' of pore water H_2S in the upper 10 to 20 cm which allows sulfide to accumulate (Fig. 9) and slows down benthic sulfide release. This deficit is clearly seen in the porewater data on the shelf (e.g. St. 2, Fig. 3 and Bohlen et al., 2011).

The simulated sediment concentrations, including BNO_3^- and H_2S, and fluxes are in qualitative and quantitative agreement with the transient features observed at the shallow shelf station (Fig. 3). The model thus supports the idea that the observed temporal trends in BNO_3^- and H_2S are due to stagnation and an increasingly nitrate-starved *Thioploca* community. Porewater NH_4^+, SO_4^{2-} and TA concentrations change only marginally following the first few weeks of stagnation, implying that they can be applied to a steady state model (Fig. 9). As time passes, however, steady state model rates accrue uncertainty. From the decrease in NH_4^+ in our hypothetical scenario (Fig. 9), we estimate a 10 to 20 % error for the steady state rates (Table 2) if the bottom water became depleted in NO_3^- two weeks prior to fieldwork. The error increases to 30 % if it occurred four weeks previously, which is the minimum time that the bottom waters were depleted in NO_3^- prior to our fieldwork. Including the time spent on our own cruise, a value of 50 % is probably more realistic. This corresponds to the minimum uncertainty in our modeled rates and fluxes, which is similar to the natural variability in DIC fluxes used to constrain POC degradation rates (Dale et al., 2015). Given the level of bottom water variability observed in the Peruvian and Chilean OMZs, it is likely that sediment pore waters and *Thioploca* biomass continuously fluctuate depending on the prevailing redox regime in the overlying water column (Graco et al., 2001; Farías et al., 2004; Graco et al., 2007; Gutiérrez et al., 2008). Given the potential impact of DNRA on N loss by anammox, proper consideration of this temporal variability is urgently needed to derive robust regional N budgets in the ETSP.

4.5. Wider socio-economic implications

Thioploca bacteria indirectly engineer major alterations to the sediment geochemistry. When bottom water NO_3^- becomes depleted due to stagnation, several months are required for benthic NH_4^+ and H_2S fluxes to equilibrate because DNRA charges the pore waters with NH_4^+ and depletes them in H_2S. This microbial legacy could have important implications for ecosystem functioning along the Peruvian margin. It implies that *Thioploca* can sustain pelagic anammox and mitigate toxic sulfide release long after the bottom water stagnates. In 2008 the largest sulfidic plume ever observed in oceanic waters (5500 km^2) occurred within continental shelf waters of the Peruvian OMZ concurrent with a lack of NO_3^- in the water column (Schunk et al., 2013). These workers identified the sediments as the source of H_2S. Given that ca. 5% of the global fish catch was landed in Peru in 2012 (http://www.fao.org), the potential socio-economic impacts of toxic sulfide accumulation in the water column are severe (Weeks

et al., 2004). Yet, such sulfidic events are relatively rare, in contrast to the highly productive Benguela upwelling system (Brüchert et al., 2006). The sulfur oxidizing bacterial community in this region is dominated by nitrate-storing *Thiomargarita* species. Being non-motile, these bacteria rely on resuspension events to recharge their nitrate reservoir (Schulz and Jørgensen, 2001), which increases the likelihood of sulfide release and mass fish mortality (Brüchert et al., 2003; Weeks et al., 2004). We suggest that buffering of sulfide flux by the porewater sulfide 'deficit' created by *Thioploca* limits the frequency of sulfidic events off Peru. Sediments at the shallowest stations may, however, act as chronic sources to the bottom water during the high productivity season. Accurate prediction of sulfide emissions requires long term monitoring of bottom water stagnation (e.g. Graco et al., 2016) and an explicit consideration of benthic DNRA in regional modeling approaches, such as ROMS (Gutknecht et al., 2013). An understanding of the causes, frequency and duration of sulfide emissions should be considered a priority area for further investigation.

ACKNOWLEDGEMENTS

We thank the captains and crew of RV Meteor and the scientific participants of cruise M92 for a friendly and professional working atmosphere on board. AD would particularly like to thank the Captain, Michael Schneider, for dealing with the authorities under extenuating circumstances. Sediment sampling and biogeochemical analyses were performed with the assistance of the ever-patient B. Domeyer, R. Suhrberg, S. Trinkler and V. Thoenissen. Preparation and deployment of large gears was performed with diligence by S. Kriwanek, A. Petersen, M. Türk, S. Cherednichenko and K. Stolpovsky. We acknowledge the diligence of two reviewers in providing constructive feedback and thank the associate editor Richard Matear for smooth handling the manuscript and a speedy review process. This work is a contribution of the Sonderforschungsbereich 754 "Climate – Biogeochemistry Interactions in the Tropical Ocean" (www.sfb754.de) which is supported by the Deutsche Forschungsgemeinschaft.

REFERENCES

1. Barnes, R. O. & Goldberg, E. D. Methane production and consumption in anoxic marine sediments. Geology 4, 297-300. 1976.
2. Bernhard, J. M., Casciotti, K. L., McIlvin, M. R., Beaudoin, D. J., Visscher, P. T., & Edgcomb , V. P. Potential importance of physiologically diverse benthic foraminifera in sedimentary nitrate storage and respiration. Journal of Geophysical Research 117, G03002, doi:10.1029/2012JG001949. 2012.
3. Bianchi, D., Dunne, J. P., Sarmiento, J. L., & Galbraith, E. D. Data-based estimates of suboxia, denitrification, and N2O production in the ocean and their sensitivities to dissolved O2. Global Biogeochemical Cycles 26, GB2009, doi:10.1029/2011GB004209. 2012.
4. Bohlen, L., Dale, A. W., Sommer, S., Mosch, T., Hensen, C., Noffke, A., Scholz, F., & Wallmann, K. Benthic nitrogen cycling traversing the Peruvian oxygen minimum zone. Geochimica et Cosmochimica Acta 75, 6094-6111. 2011.

5. Bohlen, L., Dale, A. W., & Wallmann, K. Simple transfer functions for calculating benthic fixed nitrogen losses and C:N:P regeneration ratios in global biogeochemical models. Global Biogeochemical Cycles 26, GB3029, doi:10.1029/2011GB004198. 2012.
6. Boudreau, B. P. Diagenetic Models and Their Implementation: Modelling Transport and Reactions in Aquatic Sediments, Springer-Verlag, Berlin, 414 pp. 1997.
7. Brüchert V., Currie, B., Peard, K. R., Lass, U., Endler, R., Dübecke, A., Julies, E., Leipe, T., & Zitzmann, S. An integrated assessment of shelf anoxia and water column hydrogen sulphide in the Benguela coastal upwelling system off Namibia. In Past and Present Marine Water Column Anoxia (ed. L. N. Neretin), Springer, pp. 161-194. 2006.
8. Brüchert, V., Jørgensen, B. B., Neumann, K., Riechmann, D., Schlösser, M., & Schulz, H. Regulation of bacterial sulfate reduction and hydrogen sulfide fluxes in the central Namibian coastal upwelling zone. Geochimica et Cosmochimica Acta 67, 4505-4518. 2003.
9. Burdige, D. J. Geochemistry of Marine Sediments, Princeton University Press, Princeton, 609 pp. 2006.
10. Cardich, J., Morales, M., Quipúzcoa, L., Sifeddine, A., Gutiérrez, D. Benthic foraminiferal communities and microhabitat selection on the continental shelf off central Peru. In Anoxia: Evidence for Eukaryote Survival and Paleontological Strategies. Cellular Origin, Life in Extreme Habitats and Astrobiology 21, 323–340, 2012.
11. Chong, L. S., Prokopenko, M. G., Berelson, W. M., Townsend-Small, A., & McManus, J. Nitrogen cycling within suboxic and anoxic sediments from the continental margin of Western North America. Marine Chemistry 128-129, 13-25. 2012.
12. Dale, A. W., Brüchert, V., Alperin, M., & Regnier, P. An integrated sulfur isotope model for Namibian shelf sediments. Geochimica et Cosmochimica Acta 73, 1924-1944. 2009.
13. Dale, A. W., Sommer, S., Ryabenko, E., Noffke, A., Bohlen, L., Wallmann, K., Stolpovsky, K. , Greinert, J., & Pfannkuche, O. Benthic nitrogen fluxes and fractionation of nitrate in the Mauritanian oxygen minimum zone (Eastern Tropical North Atlantic). Geochimica et Cosmochimica Acta 134, 234-256. 2014.
14. Dale, A. W., Sommer, S., Lomnitz, U., Montes, I., Treude, T., Liebetrau, V., Gier, J. , Hensen, C., Dengler, M., Stolpovsky, K., Bryant, L. D., & Wallmann, K. Organic carbon production, mineralisation and preservation on the Peruvian margin. Biogeosciences 12, 1537-1559. 2015.
15. Devol, A. H., Uhlenhopp, A. G., Naqvi, S. W. A., Brandes, J. A., Jayakumar, D. A., Naik, H., Gaurin, S., Codispoti, L. A., & Yoshinari, T. Denitrification rates and excess nitrogen gas concentrations in the Arabian Sea oxygen deficient zone. Deep Sea Research Part I: Oceanographic Research Papers 53, 1533-1547. 2006.
16. DeVries, T., Deutsch, C., Rafter, P. A., & Primeau, F. Marine denitrification rates determined from a global 3-D inverse model. Biogeosciences 10, 2481-2496, doi:10.5194/bg-10-2481-2013. 2013.
17. Eugster, O. & Gruber, N. A probabilistic estimate of global marine N-fixation and denitrification. Global Biogeochemical Cycles 26, GB4013, doi:10.1029/2012GB004300. 2012.
18. Farías, L., Graco, M., & Ulloa, O. Temporal variability of nitrogen cycling in continental-shelf sediments of the upwelling ecosystem off central Chile. Deep Sea Research Part II: Topical Studies in Oceanography 51, 2491-2505. 2004.
19. Ferdelman, T. G., Lee, C., Pantoja, S., Harder, J., Bebout, B. M., & Fossing, H. Sulfate reduction and methanogenesis in a Thioploca-dominated sediment off the coast of Chile. Geochimica et Cosmochimica Acta 61, 3065-3079. 1997.
20. Fossing, H. Sulfate reduction in shelf sediments in the upwelling region off Central Peru. Continental Shelf Research 10, 355-367. 1990.
21. Fossing, H., Gallardo, V. A., Jørgensen, B. B., Hüttel, M., Nielsen, L. P., Schulz, H., Canfield, D. E., Glud, R. N., Gundersen, J. K., Küver, J., Ramsing, N. B., Teske, A., Thamdrup, B., & Ulloa, O. Concentration and transport of nitrate by the mat-forming sulphur bacterium Thioploca. Nature 274, 713-715. 1995.
22. Galbraith, E. D., Kienast, M., Pedersen, T. F., & Calvert, S. E. Glacial-interglacial modulation of the marine nitrogen cycle by high-latitude O2 supply to the global thermocline. Global Biogeochemical Cycles 19, PA4007, doi:10.1029/2003PA001000. 2004.
23. Graco, M., Ledesma, J., Flores, G., & Giron, M. Nutrients, oxygen and biogeochemical processes in the Humboldt upwelling current system off Peru. Revista Peruana de Biologķa 14, 117-128. 2014.
24. Gallardo, V. A. Large benthic microbial communities in sulphide biota under Peru-Chile subsurface countercurrent. Nature 268, 331-332. 1977.
25. Glenn, C. R. & Arthur, M. A. Petrology and major element geochemistry of Peru margin phosphorites and associated diagenetic minerals: Authigenesis in modern organic-rich sediments. Marine Geology 80, 231-267. 1988.
26. Glock, N., Schönfeld, J., Eisenhauer, A., Hensen, C., Mallon, J., & Sommer, S. The role of benthic foraminifera in the benthic nitrogen cycle of the Peruvian oxygen minimum zone. Biogeosciences 10, 4767-4783. 2013.

27. Graco, M., Farías, L., Molina, V., Gutiérrez, D., & Nielsen, L. P. Massive developments of microbial mats following phytoplankton blooms in a naturally eutrophic bay: Implications for nitrogen cycling. Limnology and Oceanography 46, 821-532. 2001.
28. Grasshoff, K., Ehrhardt. M., Kremmling, K., 1983. Methods of Seawater Analysis. Verlag Chemie, Weinheim, 419 pp.
29. Gruber N. The dynamics of the marine nitrogen cycle and its influence on atmospheric CO_2 variations. In "Carbon-Climate Interactions", T. Oguz and M. Follows, editors, NATO ASI series. 2004.
30. Gutiérrez, D., Enríquez, E., Purca, S., Quipúzcoa, L., Marquina, R., Flores, G., & Graco, M. Oxygenation episodes on the continental shelf of central Peru: Remote forcing and benthic ecosystem response. Progress in Oceanography 79, 177-189. 2008.
31. Gutiérrez, D., Sifeddine, A., Field, D. B., Ortlieb, L., Vargas, G., Chavez, F. P., Velazco, F., Ferreira, V., Tapia, P., Salvatteci, R., Boucher, H., Morales, M. C., Valdés, J., Reyss, J.-L., Campusano, A., Boussafir, M., Mandeng-Yogo, M., Garcaa, M., & Baumgartner, T. Rapid reorganization in ocean biogeochemistry off Peru towards the end of the Little Ice Age. Biogeosciences 6, 835-848. 2009.
32. Gutknecht, E., Dadou, I., Le Vu, B., Cambon, G., Sudre, J., Garçon, V., Machu, E., Rixen, T., Kock, A., Flohr, A., Paulmier, A., and Lavik, G. (2013) Coupled physical/biogeochemical modeling including O2-dependent processes in the Eastern Boundary Upwelling Systems: application in the Benguela, Biogeosciences, 10, 3559-3591, doi:10.5194/bg-10-3559-2013.
33. Hamersley, R. M., Lavik, G., Woebken, D., Rattray, J. E., Lam, P., Hopmans, E. C., Sinninghe Damsté, J. S., Krüger, S., Graco, M., Gutiérrez, D., & Kuypers, M. M. M. Anaerobic ammonium oxidation in the Peruvian oxygen minimum zone. Limnology and Oceanography 52, 923-933. 2007.
34. Henrichs, S. M. & Farrington, J. W. Peru upwelling region sediments near 15 oS. 1. Remineralization and accumulation of organic matter. Limnology and Oceanography 29, 1-19. 1984.
35. Høgslund, S., Revsbech, N. P., Cedhagen, T., Nielsen, L. P., & Gallardo, V. A. Denitrification, nitrate turnover, and aerobic respiration by benthic foraminiferans in the oxygen minimum zone off Chile. Journal of Experimental Marine Biology and Ecology. 359, 85-91. 2008.
36. Høgslund, S., Revsbech, N. P., Kuenen, J. G., Jørgensen, B. B., Gallardo, V. A., van de Vossenberg, J., Nielsen, J. L., Holmkvist, L., Arning, E. T., & Nielsen, L. P. Physiology and behaviour of marine Thioploca. The ISME Journal 3, 647-657. 2009.
37. Huettel, M., Forster, S., Kloser, S., & Fossing, H. Vertical migration in the sediment-dwelling sulfur bacteria Thioploca spp. in overcoming diffusion limitations. Applied and Environmental Microbiology 62, 1863-1872. 1996.
38. Jørgensen, B. B. & Gallardo, V. A. *Thioploca* spp: filamentous sulfur bacteria with nitrate vacuoles. FEMS Microbiology Ecology 28, 301-313. 1999.
39. Joye, S. B. & Anderson, I. C. Nitrogen cycling in coastal sediments. In Nitrogen in the Marine Environment (2nd edition) Capone, Bronk, Mulholland and Carpenter (eds.). p 867-915. 2008.
40. Kalvelage, T., Lavik, G., Lam, P., Contreras, S., Arteaga, L., Löscher, C. R., Oschlies, A., Paulmier, A., Stramma, L., & Kuypers, M. M. M. Nitrogen cycling driven by organic matter export in the South Pacific oxygen minimum zone. Nature Geoscience 6, 228-234. 2013.
41. Koho, K. A., Piña-Ochoa, E., Geslin, E., & Risgaard-Petersen, N. Vertical migration, nitrate uptake and denitrification: survival mechanisms of foraminifers (Globobulimina turgida)under low oxygen conditions. FEMS Microbiology Ecology 75, 273-283. 2011.
42. Lam, P. & Kuypers, M. M. M. Microbial nitrogen cycling processes in oxygen minimum zones. Annual Review of Marine Science 3, 317-345. 2011.
43. Lam, P., Lavik, G., Jensen, M. M., van de Vossenberg, J., Schmid, M., Woebken, D., Gutiérrez, D., Amann, R., & Jetten, M. S. M. K. M. M. M. Revising the nitrogen cycle in the Peruvian oxygen minimum zone. Proceedings of the National Academy of Sciences of the United States of America. 106, 4752-4757. 2009.
44. Levin, L. A. Oxygen minimum zone benthos: adaptation and community response to hypoxia. Oceanography and Marine Biology: an Annual Review 41, 1-45. 2003.
45. Levin, L., Gutiérrez, D., Rathburn, A., Neira, C., Sellanes, J., Muñoz, P., Gallardo, V., & Salamanca, M. Benthic processes on the Peru margin: a transect across the oxygen minimum zone during the 1997–98 El Niño. Progress in Oceanography 53, 1-27. 2002.
46. Lichtschlag, A., Felden, J., Brüchert, V., Boetius, A., de Beer, D. Geochemical processes and chemosynthetic primary production in different thiotrophic mats of the Håkon Mosby Mud Volcano (Barents Sea). Limnology and Oceanography 55, 931-949. 2010.
47. Lomstein, E., Jensen, M. H., & Sørensen, J. Intracellular NH_4^+ and NO_3^- pools associated with deposited phytoplankton in a marine sediment (Aarhus Bright, Denmark). Marine Ecology Progress Series 61, 97-105. 1990.

48. Mackin, J. E., Aller, R. C. Ammonium adsorption in marine sediments. Limnology and Oceanography 29, 250-257. 1984
49. Maier, S. Gallardo, V. A. *Thioploca araucae* sp. nov. and *Thioploca chileae* sp. nov. International Journal of Systematic and Evolutionary Microbiology 34, 414-418. 1984.
50. Maltby, J., Sommer, S., Dale, A. W., Treude, T. Microbial methanogenesis in the sulfate-reducing zone of surface sediments traversing the Peruvian margin, Biogeosciences, 13, 283-299, 2015.
51. Middelburg, J. J., Soetaert, K., Herman, P. M. J., & Heip, C. H. R. Denitrification in marine sediments: A model study. Global Biogeochemical Cycles 10, 661-673. 1996.
52. Morales, C. E., Hormazabal, S. E., & Blanco, J. L. Interannual variability in the mesoscale distribution of the depth of the upper boundary of the oxygen minimum layer off northern Chile (18-24S): Implications for the pelagic system and biogeochemical cycling. Journal of Marine Research 57, 909-932. 1999.
53. Mosch, T., Sommer, S., Dengler, M., Noffke, A., Bohlen, L., Pfannkuche, O., Liebetrau, V., & Wallmann, K. Factors influencing the distribution of epibenthic megafauna across the Peruvian oxygen minimum zone. Deep Sea Research Part I: Oceanographic Research Papers 68, 123-135. 2012.
54. Noffke, A., Hensen, C., Sommer, S., Scholz, F., Bohlen, L., Mosch, T., Graco, M., & Wallmann, K. Benthic iron and phosphorus fluxes across the Peruvian oxygen minimum zone. Limnology and Oceanography 57, 851-867. 2012.
55. Otte, S., Kuenen, J. G., Nielsen, L. P., Paerl, H. W., Zopfi, J., Schulz, H. N., Teske, A., Strotmann, B., Gallardo, V. A., & Jørgensen, B. B. Nitrogen, carbon, and sulfur metabolism in natural Thioploca samples. Applied and Environmental Microbiology 65, 3148-3157. 1999.
56. Pennington, J. T., Mahoney K. L., Kuwahara V. S., Kolber D. D., Calienes R. & Chavez F. P. Primary production in the eastern tropical Pacific: a review. Progress in Oceanography 69, 285–317. 2006.
57. Piña-Ochoa, E., Høgslund, S., Geslin, E., Cedhagen, T., Revsbech, N. P. , Nielsen, L. P., Schweizer, M., Jorissen, F., Rysgaard, S., & Risgaard-Petersen, N. Widespread occurrence of nitrate storage and denitrification among Foraminifera and Gromiida. Proceedings of the National Academy of Sciences of the United States of America. 107, 1148-1153. 2010.
58. Prokopenko, M. G., Hammond, D. E., Berelson, W. M., Bernhard, J. M., Stott, L., & Douglas, R. Nitrogen cycling in the sediments of Santa Barbara basin and Eastern Subtropical North Pacific: Nitrogen isotopes, diagenesis and possible chemosymbiosis between two lithotrophs (Thioploca and Anammox) - "riding on a glider". Earth and Planetary Science Letters 242, 186-204. 2006.
59. Prokopenko, M. G., Hirst, M. B., De Brabandere, L., Lawrence, D. J. P., Berelson, W. M., Granger, J., Chang, B. X., Dawson, S., Crane III, E. J., Chong, L., Thamdrup, B., Townsend-Small, A., & Sigman, D. M. Nitrogen losses in anoxic marine sediments driven by Thioploca–anammox bacterial consortia. Nature 500, 194-198. 2013.
60. Prokopenko, M. G., Sigman, D. M., Berelson, W. M., Hammond, D. E., Barnett, B., Chong, A., & Townsend-Small, A. Denitrification in anoxic sediments supported by biological nitrate transport. Geochimica et Cosmochimica Acta 75, 7180-7199. 2011.
61. Quiñones, R. A., Gutierrez, M. H., Daneri, G., Aguilar, D. G., Gonzalez, H. E., Chavez, F. P.: The Humboldt Current System, in: Carbon and Nutrient Fluxes in Continental Margins: A Global Synthesis, Liu, K-. K., Atkinson, L., Quiñones, R., Talaue-McManus, L. (Eds.), Springer-Verlag, Berlin, 44-64, 2010.
62. Risgaard-Petersen, N., Langezaal, A. M., Ingvardsen, S., Schmid, M., Jetten, M. S. M., & Op den Camp, H. J. M. Evidence for complete denitrification in a benthic foraminifer. Nature 443, 93-96. 2006.
63. Schippers, A. & Jørgensen, B. B. Biogeochemistry of pyrite and iron sulfide oxidation in marine sediments. Geochimica et Cosmochimica Acta 66, 85-92. 2002.
64. Scholz, F., Hensen, C., Noffke, A., Rohde, A., Liebetrau, V., & Wallmann, K. Early diagenesis of redox-sensitive trace metals in the Peru upwelling area – response to ENSO-related oxygen fluctuations in the water column. Geochimica et Cosmochimica Acta 75, 7257-7276. 2011.
65. Schulz, H. N. & Jørgensen, B. B. Big bacteria. Annual Review of Microbiology 55, 105-137. 2001.
66. Schulz, H. N., Jørgensen, B. B., Fossing, H. A., & Ramsing, N. B. Community structure of filamentous, sheath-building sulfur bacteria, Thioploca spp., off the coast of Chile. Applied and Environmental Microbiology 62, 1855-1862. 1996.
67. Schulz, H. N., Strotmann, B., Gallardo, V. A., & Jørgensen, B. B. Population study of the filamentous sulfur bacteria Thioploca spp. off the Bay of Concepcion, Chile. Marine Ecology Progress Series 200, 117-126. 2000.
68. Schunck, H., Lavik, G., Desai, D. K., Grosskopf , T., Kalvelage, T., Löscher, C. R., Paulmier, A., Contreras, S., Siegel, H., Holtappels, M., Rosenstiel, P., Schilhabel, M. B., Graco, M., Schmitz, R. A., Kuypers, M. M. M., & LaRoche, J. Giant hydrogen sulfide plume in the oxygen minimum zone off Peru supports chemolithoautotrophy. PLoS ONE 8, 118. 2013.
69. Somes, C. J., Oschlies, A., & Schmittner, A. Isotopic constraints on the pre-industrial oceanic nitrogen budget. Biogeosciences 10, 5889-5910. 2013.

70. Song, G. D., Liu, S. M., Marchant, H., Kuypers, M. M. M., & Lavik, G. Anammox, denitrification and dissimilatory nitrate reduction to ammonium in the East China Sea sediment. Biogeosciences 10, 6851-6864, doi:10.5194/bg-10-6851-2013. 2013.
71. Stramma, L., Johnson, G. C., Sprintall, J. , & Mohrholz, V. Expanding oxygen-minimum zones in the tropical oceans. Science 320, 655-658. 2008.
72. Straub, K. L., Benz, M., Schink, B., & Widdel, F. Anaerobic, nitrate-dependent microbial oxidation of ferrous iron. Applied and Environmental Microbiology 62, 1458-1460. 1996.
73. Suess, E. Phosphate regeneration from sediments of the Peru continental margin by dissolution of fish debris. Geochimica et Cosmochimica Acta 45, 577-588. 1981.
74. Thamdrup, B. New pathways and processes in the global nitrogen cycle. Annual Review of Ecology, Evolution, and Systematics 43, 407-428. 2012.
75. Thamdrup, B. & Canfield, D. E. Pathways of carbon oxidation in continental margin sediments off central Chile. Limnology and Oceanography 41, 1629-1650. 1996.
76. Weeks, S. J., Currie, B., Bakun, A., & Peard, K. R. Hydrogen sulphide eruptions in the Atlantic Ocean off southern Africa: implications of a new view based on SeaWiFS satellite imagery. Deep-Sea Research I 51, 153-172. 2004.
77. Zopfi, J., Kjaer, T., Nielsen, L. P., & Jørgensen, B. B. Ecology of Thioploca spp.: nitrate and sulfur storage in relation to chemical microgradients and influence of Thioploca spp. on the sedimentary nitrogen cycle. Applied and Environmental Microbiology 67, 5530-5537. 2001.

Table 1: Stations and instruments deployed on the Peruvian margin. Water depths were recorded from the ship's winch and bottom water temperature and dissolved oxygen were measured using a CTD.

Station	Instrument [a]	Date	Latitude (S)	Longitude (W)	Depth (m)	Temp. (°C)	O_2 [b] (°C)
1	BIGO I–II	15.01.2013	12°13.506'	77°10.793'	74	14.0	< dl
	MUC 13	11.01.2013	12°13.496'	77°10.514'	71		
	MUC 39	25.01.2013	12°13.531'	77°10.061'	72		
2	BIGO I-V	27.01.2013	12°14.898'	77°12.705'	101	13.8	< dl
	MUC 16	12.01.2013	12°14.897'	77°12.707'	103		
3	BIGO II-IV	20.01.2013	12°16.689'	77°14.995'	128	13.7	< dl
	MUC 46	27.01.2013	12°16.697'	77°15.001'	129		
4	BIGO I-I	11.01.2013	12°18.711'	77°17.803'	142	13.4	< dl
	MUC 10	09.01.2013	12°18.708'	77°17.794'	145		
5	BIGO I-IV	23.01.2013	12°21.502'	77°21.712'	195	13.0	< dl
	MUC 45	27.01.2013	12°21.491'	77°21.702'	195		
6	BIGO II-II	12.01.2013	12°23.301'	77°24.284'	244	12.0	< dl
	MUC 5	07.01.2013	12°23.329'	77°24.185'	253		
	MUC 34	23.01.2013	12°23.300'	77°24.228'	244		
7	BIGO II-I	08.01.2013	12°24.905'	77°26.295'	306	12.5	< dl
	MUC 9	08.01.2013	12°24.894'	77°26.301'	304		
	MUC 36	24.01.2013	12°25.590'	77°25.200'	297		
8	BIGO II-V	24.01.2013	12°27.207'	77°29.517'	409	10.6	< dl
	MUC 23	15.01.2013	12°27.198'	77°29.497'	407		
	MUC 24	15.01.2013	12°27.195'	77°29.483'	407		
9	BIGO II-III	16.01.2013	12°31.366'	77°34.997'	756	5.5	19
	MUC 17	13.01.2013	12°31.374'	77°35.183'	770		
10	BIGO I-III	19.01.2013	12°34.911'	77°40.365'	989	4.4	53
	MUC 28	19.01.2013	12°35.377'	77°40.975'	1024		

[a] The first Roman numeral of the BIGO code for 12°S denotes the lander used and the second to the deployment number of that lander.
[b] < dl = below detection limit (5 μM).

Table 2. Simulated N turnover rates in mmol N m^{-2} d^{-1} [a].

Description	St. 1	St. 2	St. 3	St. 4	St. 5	St. 6	St. 7	St. 8	St. 9	St. 10
Ammonification	6.5	2.9	1.7	0.84	0.50	0.47	0.38	0.20	0.27	0.14
Denitrification	0	0	0.49	0.55	0.28	0.39	0.23	0.15	0.49	0.23
Denitrification by foraminifera	0	0	0	0	0	0	1.5	1.4	0	0
Anammox	0	0	0	0.59	0	0.21	0.68	0	0.25	0.07
Nitrification	0	0	0	0	0	0	0	0	0.13	0.09
DNRA	15.6	7.0	5.5	1.2	1.5	1.1	0.06	0	0	0
Total fixed N loss	0	0	0.49	1.14	1.14	0.60	2.38	1.51	0.74	0.30
% N_2 production by denitrification	0	0	100	48	100	65	10	10	66	75
% N_2 production by anammox	0	0	0	52	0	35	29	0	34	25
% N_2 production by foraminifera	0	0	0	0	0	0	62	90	0	0

[a] Rates on the shelf (St. 1 to 5) are tentative due to stagnation of the overlying water. The uncertainty in ammonification and DNRA at these sites is estimated to be 30 to 50 % based on the transient numerical model (Section 4.4).

Table 3. Size of the biological nitrate reservoir (BNO_3^-) in the top 10 cm and the first-order decay constant for St. 1 and 3 based on the temporal decrease in BNO_3^- (Fig. 3).

Station	Date	BNO_3^- / mmol m^{-2}	Decay constant [a] / yr
1	15.01.2013	10.9	26
	25.01.2013	5.3	
3	20.01.2013	19.9	29
	27.01.2013	11.4	
5	27.01.2013	6.0	-
6	23.01.2013	23.8	-
7	24.01.2013	9.6	-
8	17.01.2013	28.2	-

[a] Calculated as $-\ln[(BNO_3^-)_{t2}/(BNO_3^-)_{t1}] / [t_2 - t_1]$, where t_1 and t_2 denote the time (yr) of the first and second sampling day at St. 1 and St. 3.

Figure captions

Fig. 1. Bottom water concentrations of nitrate, nitrite and ammonium along the margin at 12 ^{o}S. The samples were collected from CTD water sampling rosette casts (Sommer et al., submitted). Note that ammonium concentrations have been multiplied by a factor of ten for clarity.

Fig. 2. Idealized N cycle in marine sediments showing the main reactions considered in the model. Pathways of enhanced biological nitrate transport and reduction by the sulfur oxidizing bacteria *Thioploca* spp. and foraminifera are indicated. Reaction stoichiometries of pathways R_j are provided in the Supplement.

Fig. 3. Sediment porewater and solid phase distributions along 12^{o}S. Symbols and curves denote measured and modeled data, respectively. Biological nitrate (BNO_3^-) was determined at stations 1, 3, 5, 6, 7 and 8, where black and gray shading denotes replicate cores sampled at the same station (note variable depth scales). NO_3^- concentrations measured by porewater extracted by centrifugation are shown as symbols with corresponding model curves (< dl = below detection limit). Measurable bottom water NO_3^- concentrations are indicated by the axis arrows. The open symbols in the TA plot for St. 1 correspond to TA corrected for down core decrease in Ca^{2+} and Mg^{2+} (see Supplement). Replicate cores sampled at the same stations (see Table 1) are not differentiated in the figure, except for BNO_3^- and H_2S at St. 1 and 3 where the sampling dates are shown (see text). The red curves at St. 1 show the model results with the rate of DNRA set to zero, which requires much higher organic matter degradation rates (principally sulfate reduction) to simulate the NH_4^+ data.

Fig. 4. Measured (black columns) and modeled (white columns) benthic fluxes of N species, O_2 and DIC. Measured N and O_2 fluxes are from Sommer et al. (submitted), where error bars were calculated from the standard error of the slope of the concentrations inside the benthic chambers. Measured DIC fluxes were calculated from pCO_2 and TA concentrations (Dale et al., 2015). The DIC fluxes at St. 1 to 5 have been multiplied by 0.5 to fit on the scale. The green and blue shading on the NO_3^- flux denotes the NO_3^- uptake by *Thioploca* and foraminifera, respectively. Units are mmol m^{-2} d^{-1} of N or C. A measured NO_3^- flux could not be determined at St. 1 to 3 due to the absence of bottom water NO_3^- (at St. 1 and 2) and rapid consumption inside the chamber at St. 3. The modelled NO_3^- is thus theoretical and does not reflect the hydrographic situation during sampling (see text).

Fig. 5. Sulfate-ammonium porewater property-property plots using data from the shelf and the OMZ (upper 15 cm only). The solid line and equation correspond to a linear regression.

Fig. 6. Depletion of boundary concentrations of NO_3^- (black) and BNO_3^- (red) in the transient model simulation of a stagnation event on the shelf. Stagnation begins at time = 0 d. The shaded box highlights the 9 d time period for stagnation to become established.

Fig. 7. Fluxes of (a) NO_3^-, BNO_3^-, N_2 and (b) NH_4^+ and H_2S across the sediment surface before, during and after bottom water stagnation. Stagnation begins at time = 0 d. The shaded box highlights the 9 d time period for stagnation to become established. Fluxes of NO_3^- and BNO_3^- are into the sediment, whereas fluxes for the other solutes are directed to the water column. In (b), the H_2S flux responds rapidly to stagnation due to a switch from carbon respiration by NO_3^- and NO_2^- reduction (R_2, R_3, Fig. 2) to sulfate reduction (R_5). NH_4^+ and H_2S fluxes require much longer to respond to the reduction in DNRA, taking >100 d to reach quasi-steady state. The black circle in (b) denotes the flux of H_2S measured on the shelf in the absence of bottom water NO_3^- and NO_2^- (14 mmol m^{-2} d^{-1}, Sommer et al., submitted).

Fig. 8. Rates of (a) nitrate (R_2) and nitrite (R_3) reduction (mmol m^{-2} d^{-1} of N), (b) sulfate reduction (R_5, mmol m^{-2} d^{-1} of S), and (c) DNRA (R_9, mmol m^{-2} d^{-1} of N) before, during and after bottom water stagnation. Stagnation begins at time = 0 d. The shaded box highlights the 9 d time period for stagnation to become established.

Fig. 9. Porewater concentration profiles of (a) NH_4^+, (b) H_2S, (c) BNO_3^-, (d) SO_4^{2-}, and (e) TA. The red lines shows the steady state profiles prior to stagnation whereas the blue lines show data for each consecutive two weeks following the onset of stagnation. The green profiles correspond to 130 d after stagnation, when quasi-steady state fluxes have been reached.

Fig. 10. Measured concentrations of NO_3^- + NO_2^- (triangles) and H_2S (circles) inside the benthic chamber deployed at St. 3 at 128 m water depth. Open and closed symbols correspond to chamber 1 and 2, respectively. The immediate increase in H_2S once NO_3^- + NO_2^- are exhausted is entirely consistent with the rapid switch from carbon respiration by NO_3^- and NO_2^- reduction to sulfate reduction at the sediment-water interface (Fig. 7b). Similar observations were made at St. 2 (Sommer et al., submitted).

Fig. 1

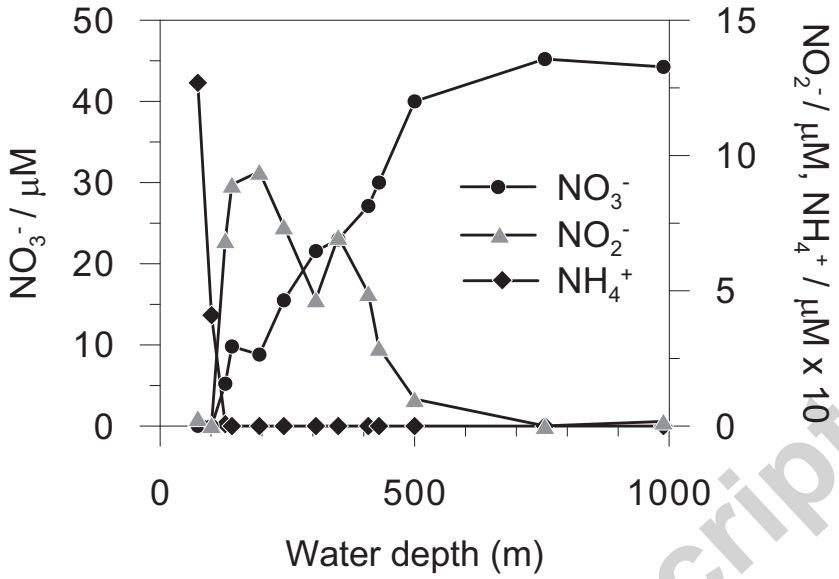
50
40
30
20
10
0
15
10
5
0
0
500
1000
Water depth (m)
NO3- / µM
NO2- / µM, NH4+ / µM x 10
NO3-
NO2-
NH4+

Fig. 2

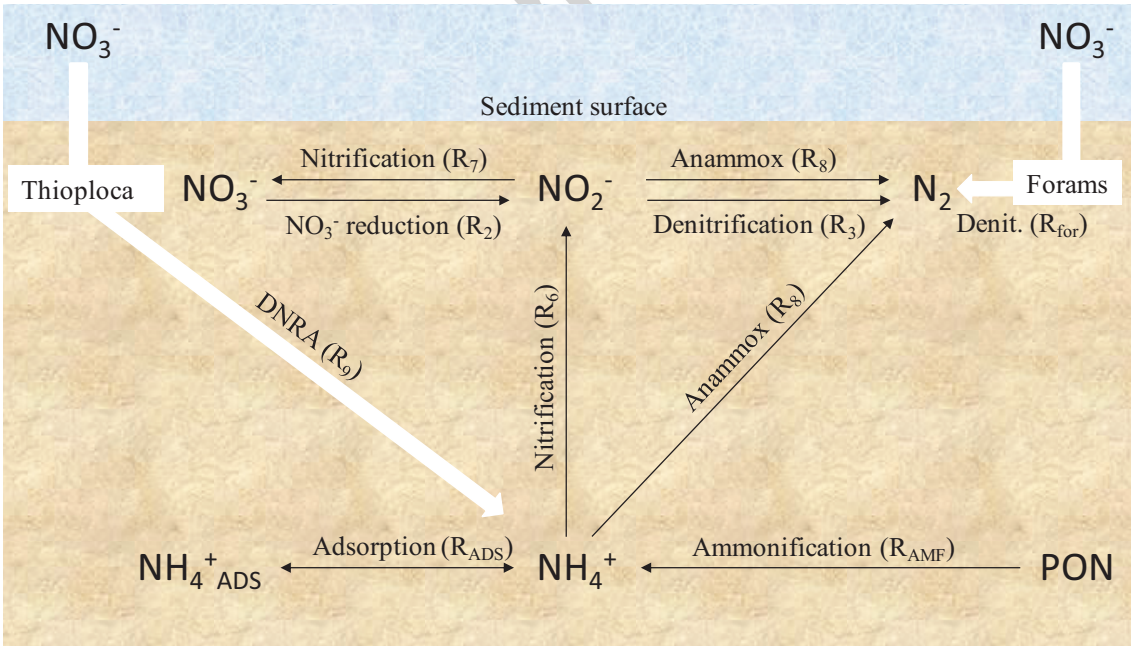
NO3-
NO3-
Sediment surface
Thioploca
NO3-
Nitrification (R7)
NO3- reduction (R2)
NO2-
Anammox (R8)
Denitrification (R3)
N2
Forams
Denit. (Rfor)
DNRA (R9)
Nitrification (R6)
Anammox (R8)
NH4+ ADS
Adsorption (RADS)
NH4+
Ammonification (RAMF)
PON

Fig. 3

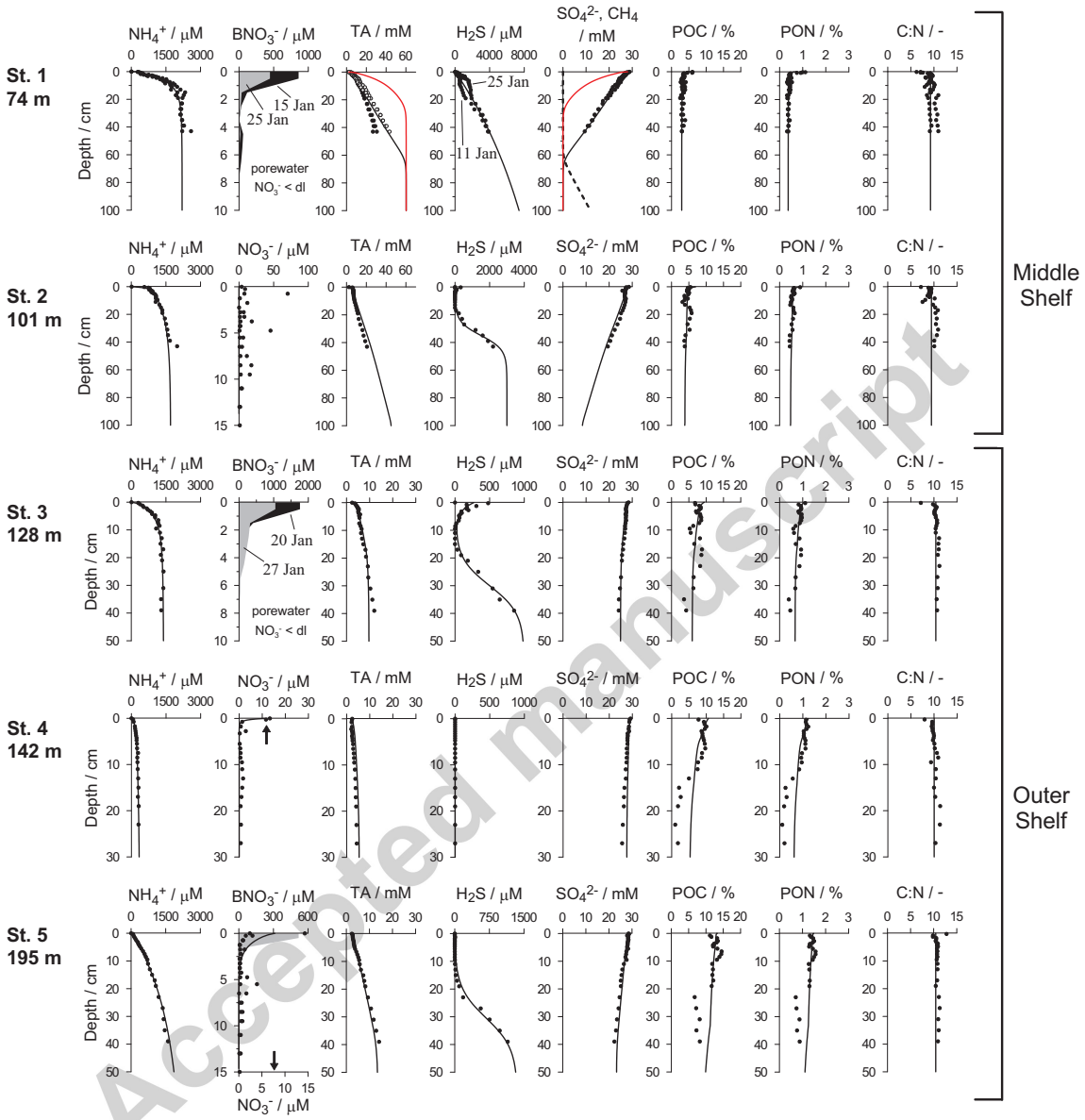

Fig. 3 continued.

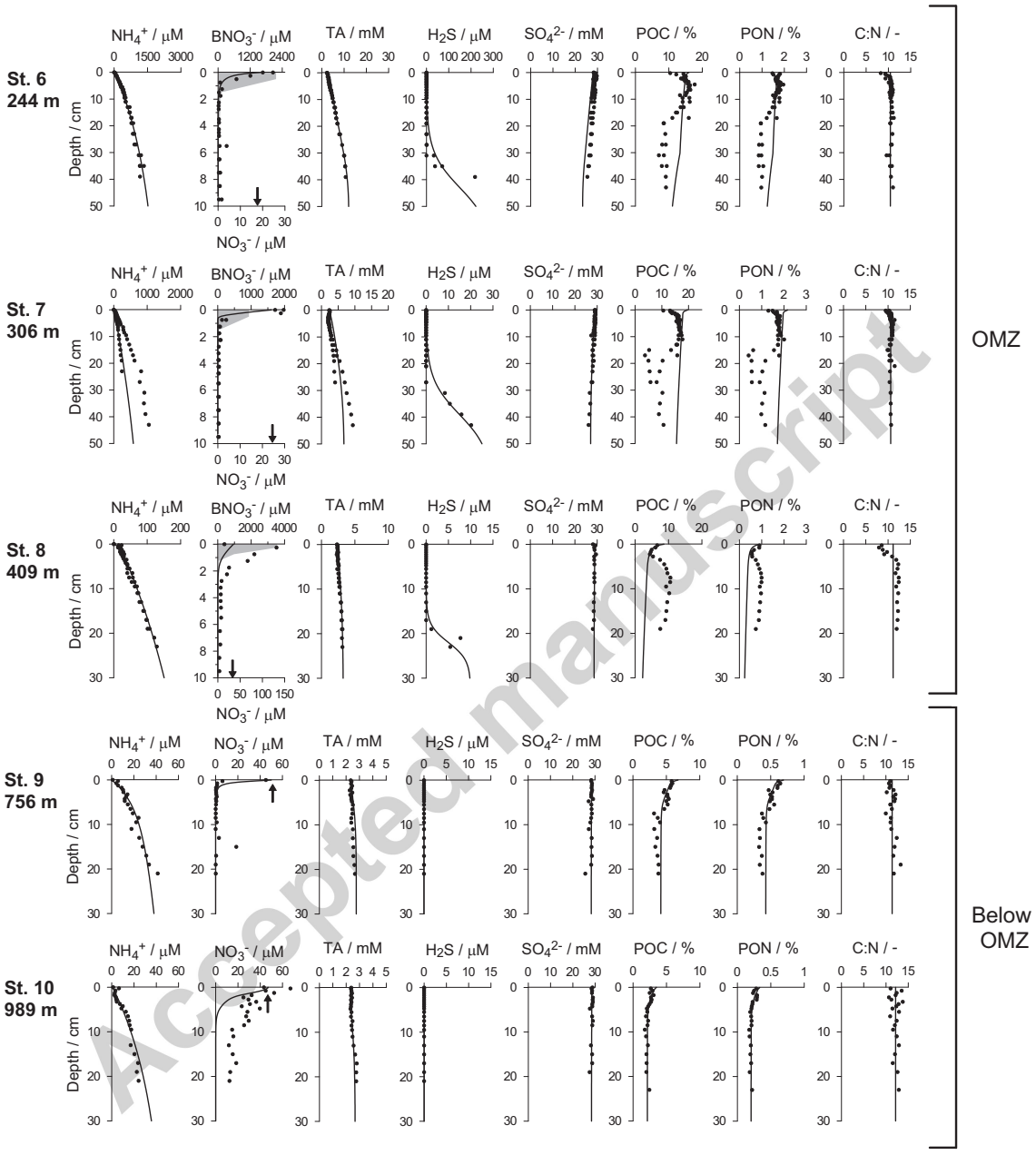

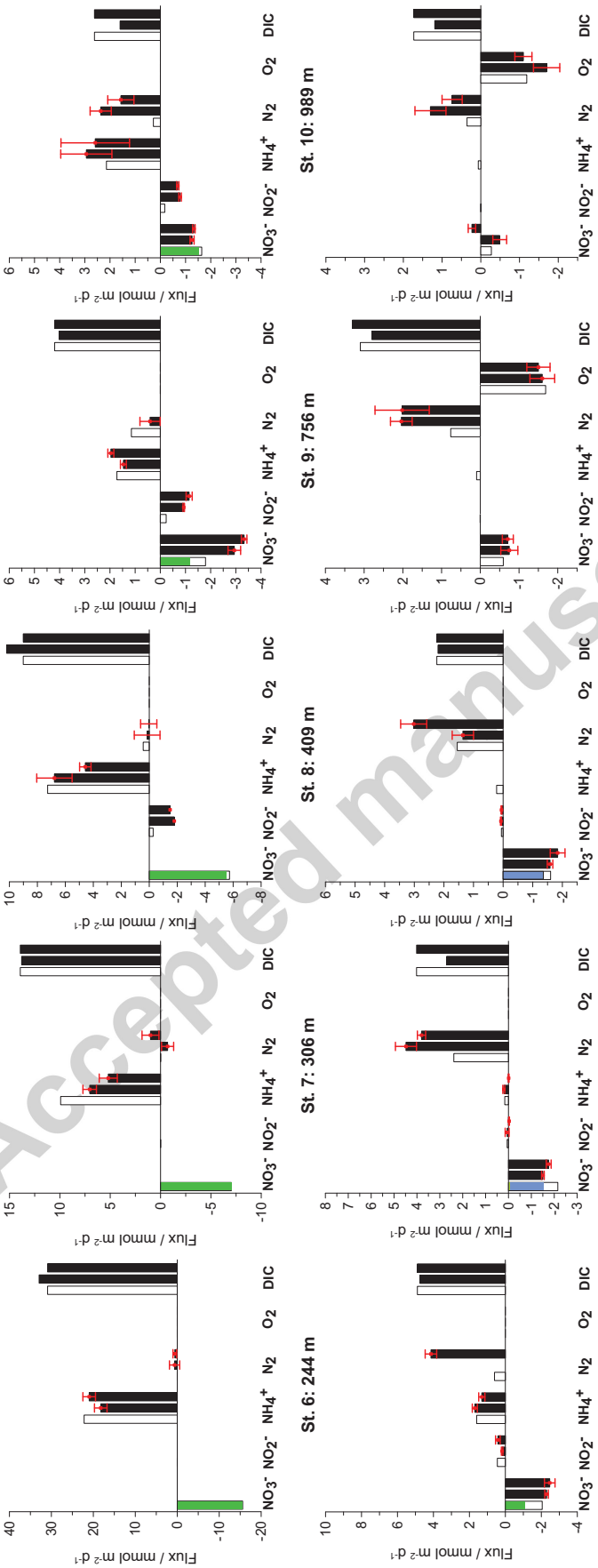

Fig. 4

Fig. 5

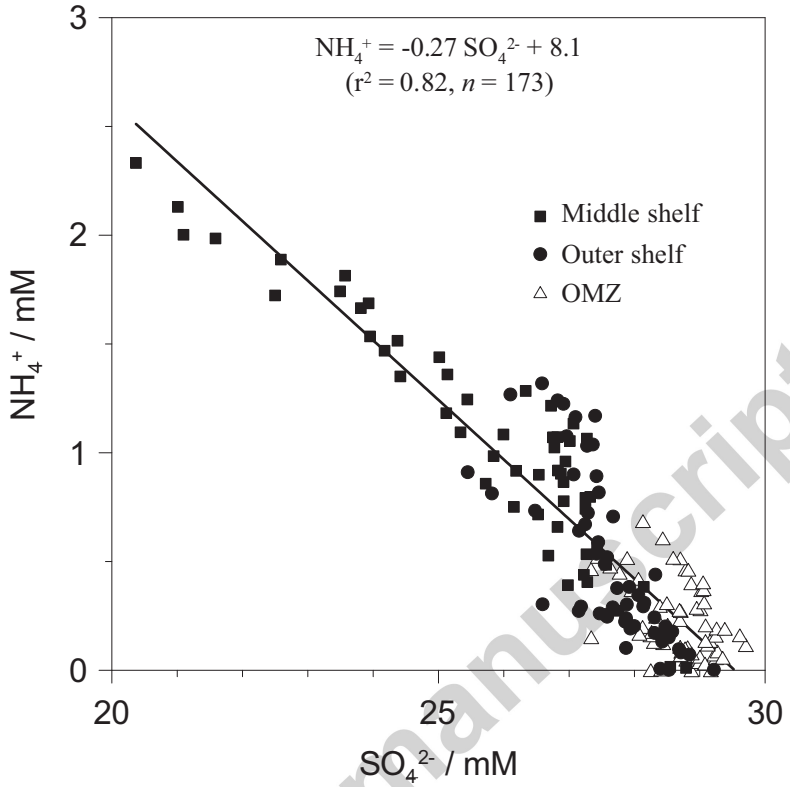

Fig. 6

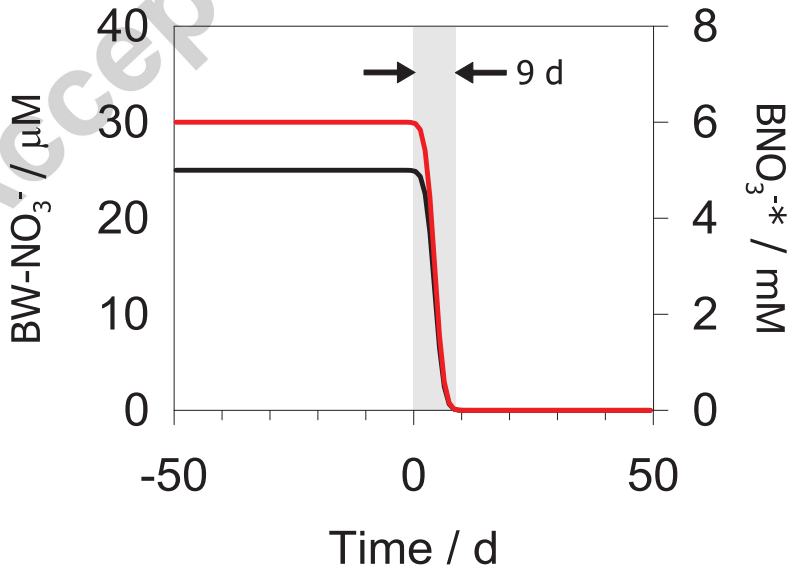

Fig. 7

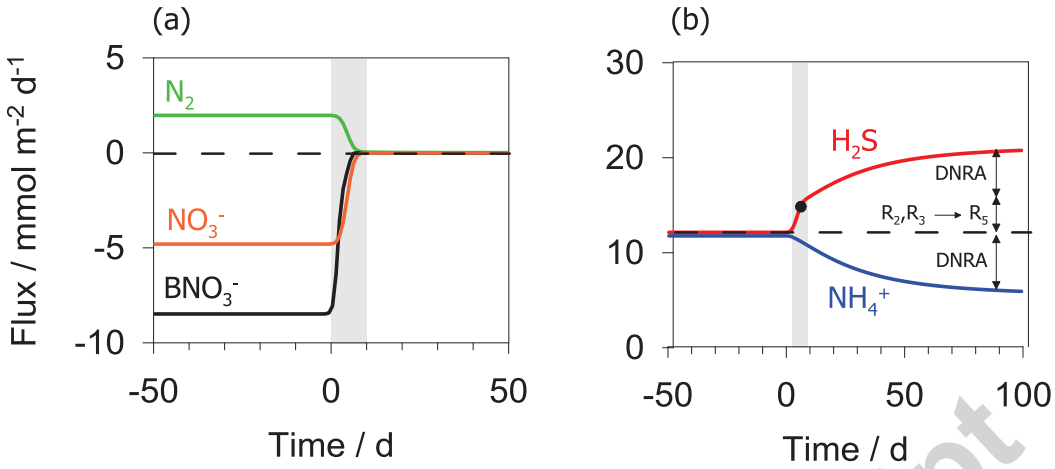

Fig. 8

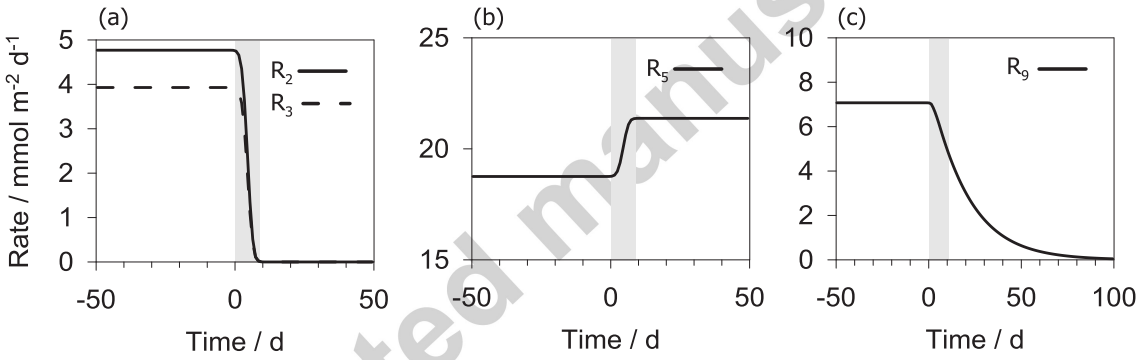

Fig. 9

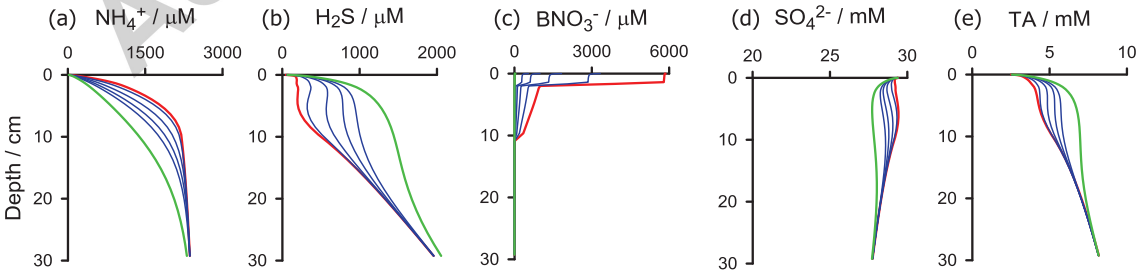

Fig. 10

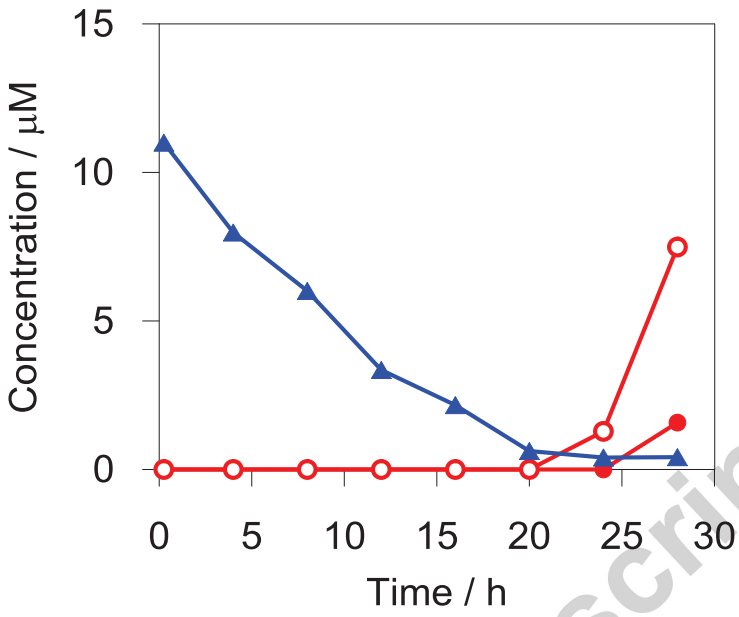

Highlights

Very high rates of dissimilatory nitrate reduction to ammonium by *Thioploca*

Non-steady state model predicts *Thioploca* survival on intracellular nitrate reservoir

Ammonium release by *Thioploca* may be coupled to pelagic N loss by anammox

Thioploca may contribute to anammox long after bottom water nitrate disappearance

Model indicates that benthic foraminifera account for 90% of benthic N_2 production